ADVANCED MATERIALS
www.advmat.de

Ultrafast and Controlled Capturing, Loading, and Release of Extracellular Vesicles by a Portable Microstructured Electrochemical Fluidic Device

*Vadim Krivitsky, Adva Krivitsky, Valeria Mantella, Maya Ben-Yehuda Greenwald, Devanarayanan Siva Sankar, Jil Betschmann, Johannes Bader, Nicole Zoratto, Kento Schreier, Sarah Feiss, Dario Walker, Jörn Dengjel, Sabine Werner, and Jean-Christophe Leroux**

Extracellular vesicles (EVs) are secreted by all living cells and are found in body fluids. They exert numerous physiological and pathological functions and serve as cargo shuttles. Due to their safety and inherent bioactivity, they have emerged as versatile therapeutic agents, biomarkers, and potential drug carriers. Despite the growing interest in EVs, current progress in this field is, in part, limited by relatively inefficient isolation techniques. Conventional methods are indeed slow, laborious, require specialized laboratory equipment, and may result in low yield and purity. This work describes an electrochemically controlled "all-in-one" device enabling capturing, loading, and releasing of EVs. The device is composed of a fluidic channel confined within antibody-coated microstructured electrodes. It rapidly isolates EVs with a high level of purity from various biofluids. As a proof of principle, the device is applied to isolate EVs from skin wounds of healthy and diabetic mice. Strikingly, it is found that EVs from healing wounds of diabetic mice are enriched in mitochondrial proteins compared to those of healthy mice. Additionally, the device improves the loading protocol of EVs with polyplexes, and may therefore find applications in nucleic acid delivery. Overall, the electrochemical device can greatly facilitate the development of EVs-based technologies.

1. Introduction

Extracellular vesicles (EVs) are naturally occurring vesicles that are secreted by all cell types and found in many body fluids, including plasma, urine, saliva, lymph, breast milk, and in tissue culture supernatant.[1] According to the International Society for Extracellular Vesicles (ISEV), the term EVs refers to a heterogeneous population of particles, ranging in size from 30 to more than 1000 nm, encompassing exosomes, microvesicles, and apoptotic bodies.[2] Similar to the plasma membrane, the membrane of EVs is composed of a phospholipid bilayer, that is highly enriched in tetraspanin proteins, such as CD9 and CD63.[3] EVs actively participate in intercellular communication by delivering nucleic acids, proteins, lipids, and small molecules to recipient cells.[4] Besides cellular signaling, EVs play a role in various biological processes like immune stimulation,

V. Krivitsky, A. Krivitsky, V. Mantella, J. Betschmann, J. Bader, N. Zoratto, K. Schreier, S. Feiss, D. Walker, J.-C. Leroux
Institute of Pharmaceutical Sciences
Department of Chemistry and Applied Biosciences
ETH Zurich
Zurich 8093, Switzerland
E-mail: jleroux@ethz.ch

M. Ben-Yehuda Greenwald, S. Werner
Institute of Molecular Health Sciences
Department of Biology
ETH Zurich
Zurich 8093, Switzerland

D. S. Sankar, J. Dengjel
Department of Biology
University of Fribourg
Fribourg 1700, Switzerland

The ORCID identification number(s) for the author(s) of this article can be found under https://doi.org/10.1002/adma.202212000

DOI: 10.1002/adma.202212000

development regulation, and control of energy metabolism.[5] As such, they are investigated as bioregenerative agents[6] and potential substitutes for cell therapy.[7] At least 120 clinical trials involving EVs are registered at the US National Institution for Health (NIH) clinical trials website, from which 23 have already been completed.[8] In addition, EVs are involved in a number of pathological processes such as diabetes, neurodegeneration, and cancer,[9] partly by "spreading" pathological messengers.[10] In this respect, EVs are emerging as promising biomarkers.[11] In particular, EVs-based "liquid biopsy" tests are already commercially available.[12] Nevertheless, despite the growing interest in developing EVs for therapeutic and diagnostic usage, progress in this field is partly hindered by relatively inefficient isolation techniques.[13] The main hurdle in the EVs isolation process is often their sparseness in the source biological fluid. Moreover, their heterogeneity further complicates their purification.[14] Common isolation methods, such as centrifugation,[15] filtration,[16] and size-exclusion chromatography[17] involve multiple time-consuming steps, lack selectivity, may retain impurities, and require specialized laboratory equipment.[18] Volume-excluding polymers can precipitate EVs, however, they also concentrate contaminants.[19] More selective isolation approaches capture EVs based on their high-affinity binding to specific antibodies. For example, some commercial kits rely on magnetic beads coated with antibodies against the common EVs surface molecules.[20] Another approach employs a paper-based antibody-modified platform.[21] Despite their high specificity, these methods have a low capacity, which limits their yield.[18] Commercially available affinity columns can be coated with antibodies against EVs' surface molecules to improve the yield. Nevertheless, this approach still requires long column preparation time and buffer exchanges.[22] Recently, microfluidics-based techniques have emerged as rapid and low-cost alternatives.[23] A herringbone chip was designed to increase EVs' interactions with antibodies, which were coated on the surface of the microfluidic channel.[24] Kinetic microfluidic strategies utilize the EVs' distinct movement under the application of an external force induced, for example, by the application of voltage.[25] These devices were combined with filtration,[26] or with immunoaffinity capturing.[27] Nonetheless, the high voltage that is required to allow EVs' migration and the charge screening effect of physiological fluids limit the size of the channel, and therefore the output.[28] Alternatively, an acoustofluidic platform was designed to separate EVs directly from blood,[26a] which was, however, limited to small volumes, and required photolithography and clean-room facility for its fabrication. In conclusion, despite the recent improvements offered by microfluidics and other emerging technologies such as the affinity-based platforms, currently available devices have limitations, such as a low sample processing capacity, narrow applicability, and limited integration with downstream therapeutic applications.[18,25c]

To overcome the various challenges associated with the isolation of EVs from native physiological fluids, we have designed a state-of-the-art electrochemically controlled capturing and release fluidic device. EVs are immobilized on the device by affinity interactions, and controllably released by applying voltage. Compared to conventional EVs isolation methods, and in particular compared to other immunoaffinity, electrokinetic, and microfluidic-based devices, the developed device allows the processing of larger sample volumes of various physiological fluids, in a significantly shorter time, at low cost and with a high level of purity. The microfluidic channel walls consist of fibrous material that increases the active surface area for functionalization while enabling faster flow rates for optimum yields. Sample handling, reagent mixing, separation, and detection are simplified. Using this device, EVs were extracted from various biofluids as well as wounded skin tissue originating from healthy and diabetic mice, revealing differences in the protein composition between both types of mice. Finally, we demonstrated that the device can be employed in nucleic acid loading protocols to purify EVs, and remove excess and potentially toxic transfection agents. The device offers an "all-in-one" lab-on-a-chip approach capable of separating EVs directly from biological fluids in a simple and efficient manner, while also allowing their subsequent manipulation.

2. Results

2.1. Operation Concept of the Portable Microstructured Electrochemical Device

The device consists of a fluidic channel confined within 3D microstructured micro-carbon fiber (μCF) electrodes embedded in a poly(dimethylsiloxane) (PDMS) matrix and connected to a potentiostat (**Figure 1**A). EVs purification and manipulation steps were performed as follows: i) The μCF surface of the fluidic channel was first modified with amines to electrostatically adsorb negatively charged capturing antibodies and form the immunoselective layer (Figure 1B). ii) The electrodes' surface was then stably coated with an antibody of choice (e.g., anti-CD9 or -CD63) by injecting them into the fluidic channel (Figure 1C). iii) The biofluid was injected into the fluidic channel, where the EVs were specifically adsorbed by immunoaffinity interactions (Figure 1D). iii) The EVs were then washed and released with a buffer of choice or deionized water (DIW) by applying a negative potential on the working electrode (WE) (Figure 1E). Several processes contribute to the release of the EVs from the antibodies: a) Electrical repulsion between the negatively charged EVs and the negative WE. b) Below −1.23 V, water molecules are subjected to electrolysis, which produces H_2 (g) and O_2 (g) on the surface of the WE and the counter electrode (CE), respectively. These gases repel the EVs and prevent re-binding. c) Local pH changes on the surface of the electrodes lead to conformational changes of the antibodies and weaken their affinity towards the EVs[29] (Figure 1H). iv) An optional loading step can be performed, for instance, of nucleic acids such as siRNA, by introducing them complexed to a transfection reagent into the fluidic channel (Figure 1F) and subsequent wash, prior to their release by the application of a negative potential (Figure 1G).

2.2. Device Components and Characterization

The EVs separation device is composed of a 3D μCF electrode bearing a high surface area embedded in a PDMS-based fluidic channel (**Figure 2**). First, two separate semi-channels

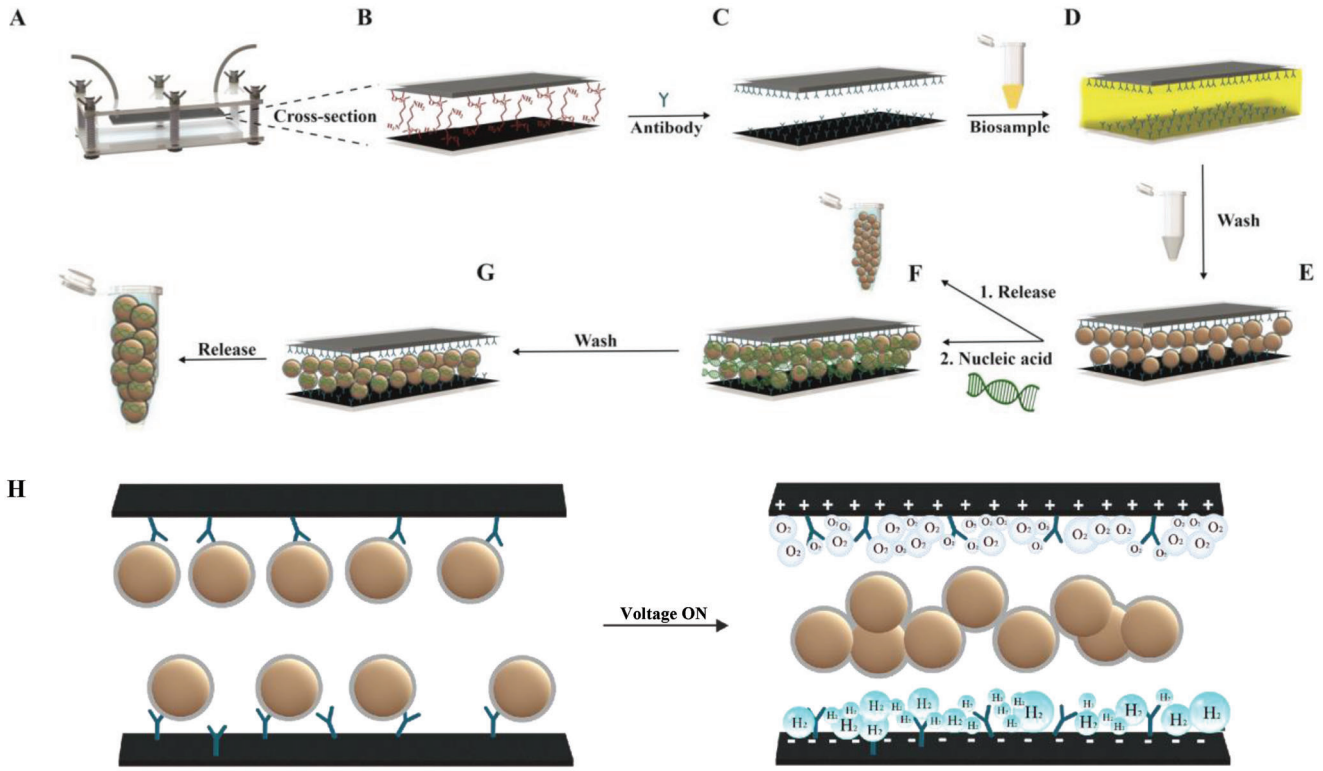

Figure 1. Schematic representation of the electrochemical device and operation process. A) Device setup, B) electrode previously modified with amino groups, C) antibody conjugation, D) biofluid injection, E) controlled release of the attached EVs by applying voltage, F) optional step-injection of transfection medium in order to form EV-nucleic acid:transfection complexes followed by a washing step, G) release of the loaded EVs by applying voltage. H) Release mechanism of the EVs from the electrodes' surface.

were fabricated using molding as detailed in Figure 2A and Figure S1 (Supporting Information). After casting the PDMS into the mold (Figure 2A), the semi-channels were activated in plasma (Figure 2B), and immediately modified with 3-aminopropyldimethylethoxysilane (APDMES) in a vacuum oven to introduce amine groups on the electrode surface (Figure 2C).[30] The capturing and release unit included the μCF electrodes and the PDMS flow cell that together confined the fluidic channel (Figure 2D). Each semi-channel has a depth of 100 μm (Figure 2E and Figure S1D, Supporting Information), and together they construct a 200 μm-wide fluidic channel. Energy-dispersive X-ray spectroscopy (EDX) mapping of the semi-channel's cross-section confirmed that the sponge-like structure of the μCF electrode is largely devoid of PDMS, and is available for antibody attachment (Figure 2F). The "noodle-like" structure of the μCF electrodes, bearing fibers with diameters of 5–10 μm, confers a large surface area for antibody immobilization[30–31] (Figure 2G). Furthermore, surface-enhanced Raman spectroscopy (SERS) confirmed the introduction of amine and siloxane groups to the electrodes' surface (Figure 2H). This is in accordance with previous publications showing similar surface APDMES modification.[30,32] The semi-channels were held together between two transparent poly(methyl methacrylate) (PMMA) sheets and tightened with screws to prevent leaks (Figure 2I,J). Following assembly, a quality check was performed to detect: 1) short circuits, which occur when the CE and the WE touch each other and the current is not passing through the solution; 2) leaks, which would reduce the amount of the captured EVs. The first five cycles of cyclic voltammetry, performed between −0.1 V and +0.1 V, confirmed the stability of the system, and produced a current in the μA range, indicating that the channel was not blocked, and that there were no short circuits (Figure 2K). The activated surface of the electrodes was coated with antibodies by injecting them into the fluidic channel. The antibodies adsorbed on the surface within a few min (Figure S2A, Supporting Information). The most cost-effective amount of antibodies required for the modification was 6.4 μg, which separated $\approx 3 \times 10^9$ vesicles mL^{-1}. A device modified with 10 times less anti-CD9 antibody captured only $\approx 5 \times 10^7$ EVs mL^{-1} (Figure S2B, Supporting Information). Separations performed with non-specific antibodies (anti-BSA and anti-TSG101), yielded $\approx 10^8$ nanoparticles mL^{-1} (Figure S2C, Supporting Information). Then, the fluidic channel was washed with 20 mL of phosphate buffer saline (PBS), which is sufficient to remove loosely bound antibodies (Figure S2D, Supporting Information). Inlet and outlet tubes connected the fluidic channel to the syringes allowing to manually inject the sample from one end while collecting the purified EVs from the other end. Crocodile clips were used to connect the potentiostat to the μCF electrodes. This was done via three needles that were inserted through the PDMS layer, to form a three-electrode electrochemical cell setup, including a WE, a CE, and a reference electrode (RE) (Figure 2I,J).

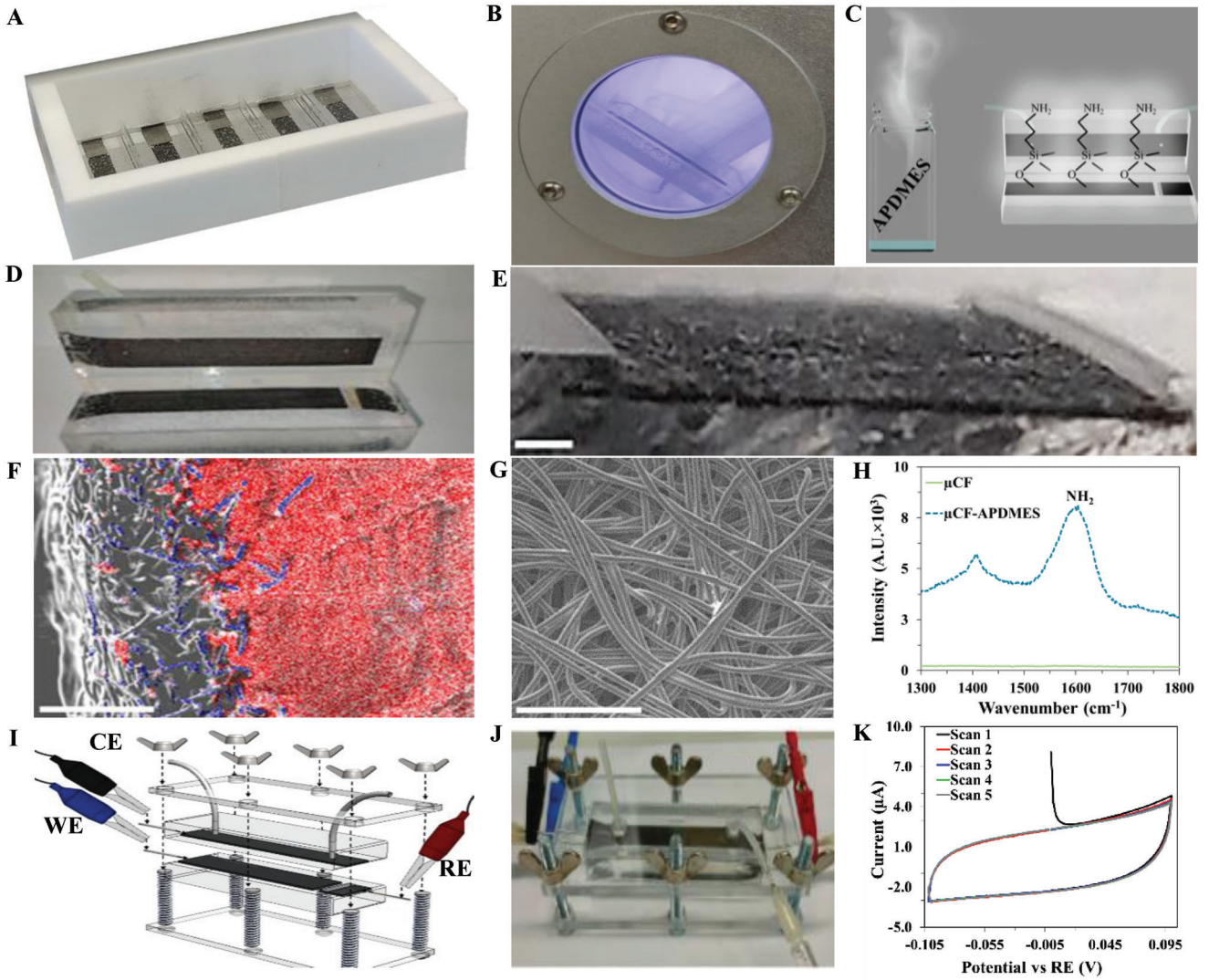

Figure 2. Assembly and performance characterization of the μCF electrochemical device. A) Image of the molds used for casting the PDMS and forming the two semi-channels. B) Electrodes' surface activation in oxygen plasma. C) Gas-phase modification with APDMES to introduce amines on the surface of the electrodes. D) Image of the two semi-channels that together form the fluidic channel. E) Cross-section of the fluidic semi-channel demonstrating the μCF embedded into the PDMS, as obtained by a DMI6000 Leica microscope. Scale bar: 200 μm. F) EDX mapping from the cross-section of the device. Blue: carbon atoms; Red: silicone atoms. Scale bar: 200 μm. G) Scanning electron microscopy (SEM) image of a bare μCF electrode, as obtained by a secondary-electron detector at an acceleration voltage of 10 kV. Scale bar: 200 μm. H) Raman spectroscopy demonstrates the introduction of amine and siloxane groups to the surface of the carbon electrodes. I) Composition scheme of the device, bearing a disposable capturing and release unit that is assembled from two parts of the fluidic channel, tightened together and held between two PMMA lids, and tightened with six bolts and nuts. An inlet and outlet tubes allow sample injection and withdrawal. A three-electrode electrochemical cell is created inside the fluidic channel by connecting the μCF electrodes to the potentiostat via steel needles. The blue crocodile clip is connected to the WE, the black crocodile clip is connected to the CE, and the red crocodile clip is connected to the RE. J) Image of the assembled device. K) Cyclic voltammetry quality check of the assembled electrochemical system. The first five cycles, performed in PBS with a scan rate of 0.02 V s^{-1} in the range of −0.1 to 0.1 V and a step of 0.002 V, confirm the stability of the electrochemical system.

2.3. Morphology, Enzymatic Activity, and Protein Markers Characterization of the Purified EVs

The EVs' separation device was first tested on human urine samples. Urine contains a large amount of EVs that are secreted mainly from the bladder tissue, urethra, and renal epithelial cells.[33] It can be non-invasively and easily collected in large volumes. Numerous publications have linked kidney diseases, prostate and bladder cancers, and even Parkinson's disease and systemic lupus, to the abundance of proteins in urinary EVs.[34] While most current EVs separation methods recommend initial centrifugation steps of the urine samples to remove large contaminants,[35] our method enabled to directly inject 50 mL of raw urine into the fluidic channel. Samples were then pushed back and forth 10 times through the fluidic channel within the course of 10 min. This step promoted interactions with the immunoaffinity layer and increased the number of collected vesicles, without affecting their size distribution (Figure S2E,

Supporting Information). Either anti-CD9 or anti-CD63 antibodies were employed as the attachment layer for EVs isolation experiments. Purified vesicles were released into 1 mL of DIW, for western blot analysis, or into 1 mL of PBS, for TEM or SEM analysis, by the application of −1.5 V. This voltage produces repulsive energy, which is approximately 2 times larger than the energy of the complex between the EVs and the coating antibodies, and experimentally found to release the largest number of vesicles without the undesired release of the antibody (Figure S2F,G, Supporting Information). The low amount of antibody that is released with the EVs, upon potential (−1.5 V), was confirmed by nanoflow cytometry (NanoFCM). EVs that were first purified from the bone marrow mesenchymal stromal cell (MSC) line HS-5 culture medium by ultracentrifugation, were subjected to a second purification step with the device. Only 5% of the released EVs were positive for the surface antibody, indicating that a small vesicle fraction carried the released antibodies (Figure S3, Supporting Information). Using these settings, we obtained capturing efficiency and recovery rates that were above ≈70% and up to ≈95%, respectively (Figure S2H,I, Supporting Information). Western blot analysis of purified urinary EVs revealed the presence of the membrane-attached tetraspanin CD9, regardless of the antibody used for the affinity layer (**Figure 3**A),[36] and also the presence of CD63 (Figure S4A, Supporting Information). The cytosolic marker tumor susceptibility gene 101 (TSG101) was also detected in both isolated populations. As a control, raw urine was loaded on the gel at normalized protein amounts. This sample did not show the EVs-associated proteins TSG101 and CD9. However, it contained high levels of albumin, while EVs isolated with anti-CD9 surface modification were largely devoid of it. SEM and TEM images showed a field of spherical particles (Figure 3C,D), demonstrating, in large magnification, the typical cup-shaped morphology (Figure S4C, Supporting Information).[37] The structure of the phospholipid bilayer membrane could be observed by cryo-TEM[37] (Figure 3F).

To further demonstrate the versatility of the device, EVs were isolated from human serum or plasma. 10 mL of raw serum were injected into the fluidic channel and pushed back and forth 10 times, as in the urine isolation experiment. The purified EVs were released into 1 mL of DIW by the application of −1.5 V. Typical CD9 and TSG101 bands were observed in the western blots. In comparison with the raw serum that was used as a control, EVs isolated using anti-CD9 as the immunoaffinity layer were largely devoid of IgG, demonstrating the high specificity that could be achieved with our separation method in comparison with conventional isolation techniques (Figure 3B and Figure S4B, Supporting Information).[39] With the anti-CD63, the purification revealed, however, less efficient, but it can potentially be improved by prolonging the washing step. Plasma EVs separated by a similar method displayed the typical vesicular morphology, as shown by SEM and cryo-TEM (Figure 3E,G). The impact of the isolation procedure on the enzymatic activity of EVs derived from HS-5 cells was further investigated. Therefore, the enzymatic activity of the membrane-bound ectonucleotidase CD73, an important regulator of local immune responses, was measured.[40] Initially, it was verified that EVs isolated from the culture medium of HS-5 cells express CD73 (Figure S4D, Supporting Information). Notably, HS-5-derived EVs isolated by ultracentrifugation revealed similar CD73 enzymatic activity before and after the subsequent purification via the anti-CD9-modified device. This result suggests that purification by the device does not impair the activity of important EVs-associated proteins (Figure 3H,I). Furthermore, EVs isolated with an anti-CD73 coated device, revealed a higher CD73 enzymatic activity compared with the first step of isolation by ultracentrifugation or with the anti-CD9 coated device, further demonstrating the high specificity towards a selected sub-population of EVs. Finally, the potential reusability of the device was demonstrated. Similar populations of EVs were isolated from HeLa-GFP cell culture medium using a single device in 3 subsequent separations. Furthermore, a single device was used to separate EVs on 3 separate days, applying a simple process of disassembly, surface activation, and coating with antibodies in between (Figure S5, Supporting Information).

2.4. Nanoparticle Tracking Analysis (NTA) of Purified EVs

Next, the separated EVs from various biofluids were analyzed for their size distribution and concentration using NTA. EVs from urine had average median sizes of 92 ± 3 and 141 ± 2 nm when captured with the anti-CD9 or anti-CD63 antibodies, respectively (**Figure 4**A). EVs separated from HeLa-GFP cell culture medium using the anti-CD9 and anti-CD63 antibodies had median sizes of 118 ± 3 and 138 ± 3 nm (Figure 4D), from serum of 114 ± 3 and 116 ± 3 nm (Figure S6, Supporting Information) and from human plasma of 131 ± 3 and 86 ± 7 nm (Figure 4G), respectively. Notably, all EVs populations separated with the device using either CD9 or CD63 immuno-modification exhibited a narrower size distribution compared with the corresponding population separated by ultracentrifugation (Figure 4B,E,H). The percentage of vesicles with a size below 200 nm was much higher in all EVs populations purified with the device compared with ultracentrifugation. The device's specificity in this regard was ≈90% when modified with an anti-CD9 antibody and between 80% and 95% with the anti-CD63 antibody, for the three types of separation media (urine, cell culture medium, and plasma) (Figure 4C,F,I). To conclude, all EVs populations separated by the device displayed the typical size distribution between 30 and 200 nm.[41] The amount of EVs recovered from plasma and serum using the anti-CD9 modified electrode was larger compared to urine and cell culture media, in accordance with previous reports.[42] Purification with the anti-CD63 antibody resulted in a lower amount of EVs compared to the anti-CD9 separation in all samples (3.4×10^8 to 8.2×10^9 particles). This can be explained by the fact that CD9 is a common EVs marker for all sub-populations, which include endosomes and plasma membrane-derived vesicles, while CD63 is typical for EVs originating from the endosomal pathway.[36a,43] This indicates that the device in its current configuration could be further used for an estimation of the abundance of EVs subpopulations in the investigated media, simply by changing the type of the attached antibody.

2.5. Isolation of EVs from Skin Wounds

In order to further test the device, it was used to isolate EVs from murine excisional skin wounds. These acute wounds normally heal within 1–2 weeks after injury[44] through a complex and dynamic process that also involves the secretion of EVs.[45] Indeed,

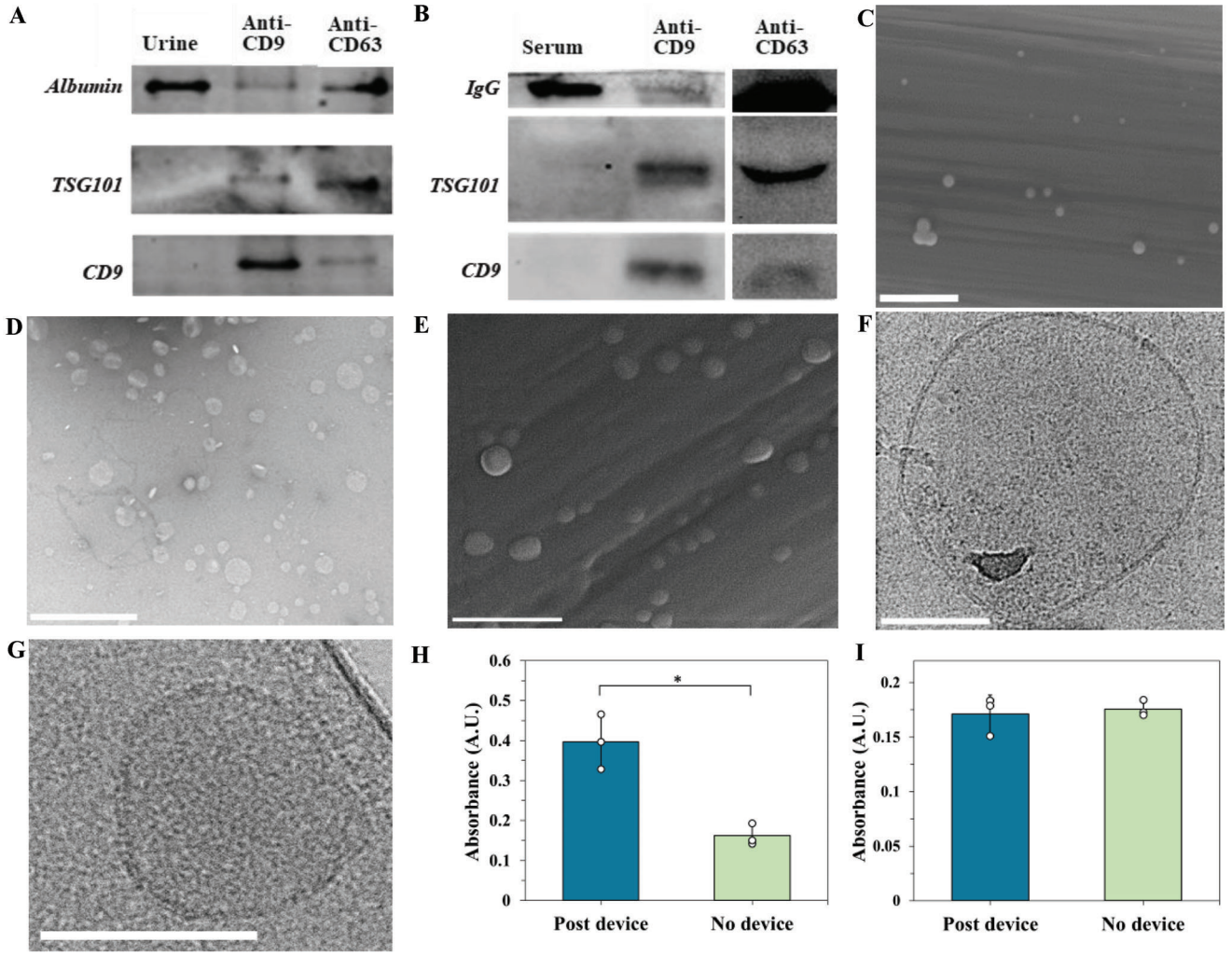

Figure 3. Characterization of the purified EVs. A,B) Western blot analysis. A) EVs separated from urine using either anti-CD9 (second lane) or anti-CD63 (third lane) immunoaffinity layer contained the protein markers CD9 (membrane protein) and TSG101 (soluble) and were largely devoid of albumin in comparison with raw urine (first lane). B) EVs separated from serum using either anti-CD9 (second lane) or anti-CD63 (third lane) contained CD9 and TSG101. IgG was used as a protein marker that is highly abundant in serum. C) SEM image of a field of urinary EVs purified using a device with an anti-CD63 immunoaffinity layer. Scale bar: 2 µm. D) Low magnification TEM image of a field of EVs separated from urine with an anti-CD63 immunoaffinity layer and negatively stained with uranyl acetate. Scale bar: 500 nm. E) SEM image of a field of serum EVs purified using a device with an anti-CD9 immunoaffinity layer. Scale bar: 500 nm. F) Large magnification cryo-TEM image of a single EV purified from urine with an anti-CD9 immunoaffinity layer. Scale bar: 100 nm. G) Large magnification cryo-TEM image of a single EV purified from human plasma with an anti-CD9 immunoaffinity layer. Scale bar: 100 nm. H–I) Enzymatic activity of EVs proteins after further purification with the device. EVs were isolated from HS-5 cell culture supernatant by ultracentrifugation, then purified again either with anti-CD73, $*p = 0.016$ (H) or with anti-CD9 modified device (I) (mean ± SD, $n = 3$). CD73 enzymatic activity was measured by the addition of malachite green.[38]

the latter were shown to play a pivotal role in cutaneous wound repair via paracrine and endocrine mechanisms, affecting different cell types.[15,45] Unfortunately, in patients suffering from pathologies such as diabetes mellitus, the wound-healing process is disturbed, frequently resulting in the development of ulcerative skin defects (chronic wounds).[44b,c] Healing of these wounds may be promoted by EVs through various mechanisms.[46] In efforts to gain first insight into EVs' role in diabetic wounds, we separated and characterized wound-secreted EVs from genetically diabetic db/db mice, which show delayed wound healing,[47] and from healthy control mice. Mice were sacrificed on day 7 post-wounding. Wounds were excised and incubated in PBS for 10 min at 37 °C to allow EVs release from the tissues (Figure S7B, Supporting Information). The collection medium was injected into the fluidic channel and EVs were purified using the anti-CD9 antibody (**Figure 5**A). NTA analysis demonstrated that EVs could be isolated in good yields from the incubation medium (Figure 5B,C). Next, we compared the concentration and size of EVs recovered from wounds in both healthy and diabetic mice. While the size distribution of the separated EVs was similar between both groups (≈128 and ≈123 nm, respectively), a trend towards a higher concentration was observed in the diabetic group compared with the healthy group ($2.6 \times 10^9 \pm 1.2 \times 10^9$ EVs mL^{-1} vs $4.3 \times 10^8 \pm 7.27 \times 10^7$ EVs mL^{-1}; Figure 5B,C and

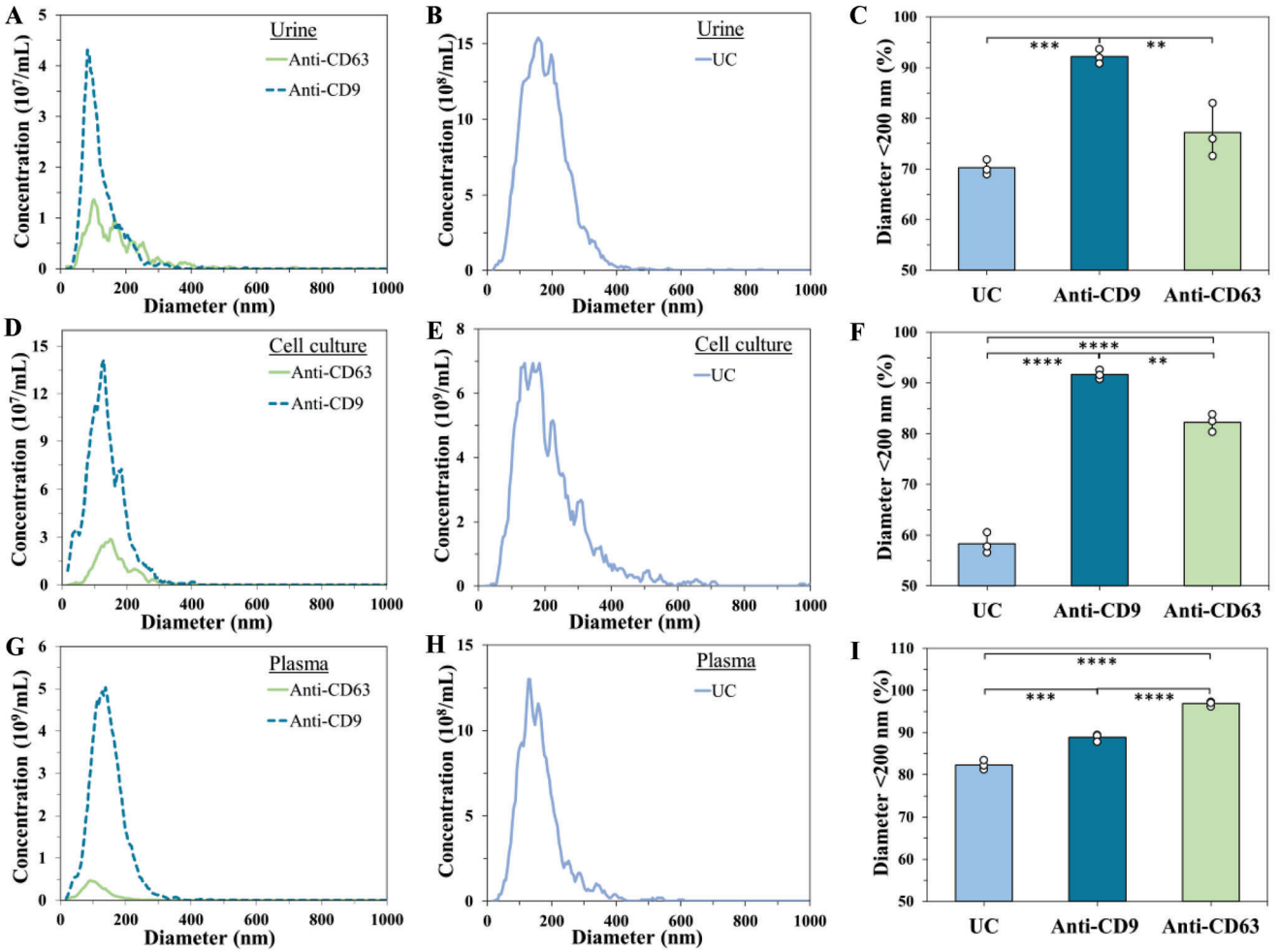

Figure 4. A,B,D,E,G,H) NTA plots of purified EVs separated with anti-CD9 (dashed cyan line) or anti-CD63 (green line) modified device from urine (A), cell culture (D), and plasma (G), vs separation from the corresponding physiological fluid by ultracentrifugation (B,E,H). C,F,I) The percentage of particles <200 nm isolated from urine (***p = 0.0005 UC vs Anti-CD9, **p = 0.003 Anti-CD9 vs Anti-CD63) (C), cell-culture medium (****p = 0.000001 UC vs Anti-CD9, ****p = 0.000005 UC vs Anti-CD63, **p = 0.001 Anti-CD9 vs Anti-CD63) (F), and plasma (***p = 0.0002 UC vs Anti-CD9, ****p = 0.000002 UC vs Anti-CD63, ****p = 0.00008 Anti-CD9 vs Anti-CD63) (I) using ultracentrifugation or a device modified with anti-CD9 or anti-CD63 antibodies (mean ± SD, n = 3). All data were smoothed by moving average trendline (period = 4).

Figure S7A, Supporting Information). This corroborates previously published data reporting an increased number of circulating EVs in metabolically unhealthy obese patients compared with healthy individuals.[48] This phenomenon of disease-related increased EVs secretion was also reported in cancer, inflammation, and liver diseases.[49] It should be considered, however, that the healing process was less advanced in the diabetic wounds and therefore, the increased amounts of EVs isolated from these wounds may also reflect the different stages of healing. This should be tested in the future using EVs harvested from wounds at different time points. Next, the proteomic profiles of the wound EVs were analyzed. We performed classical bottom-up proteomics coupled to label-free quantification of fragment spectra based on Data-Independent-Analysis (DIA) and characterized the proteomes of the isolated vesicles. The EVs populations of diabetic and WT mice could be clearly separated by a principal component analysis reflecting the variation between protein abundances of the different samples (Figure 5D; Figure S7C,D, Supporting Information). Thus, the proteomes of EVs from diabetic and WT mice differed on a global scale. In total, 1681 proteins were quantified, of which 124 showed significant abundance differences between the two groups (two-sample unpaired t-test, FDR<0.05, 65 enriched in diabetic and 59 in WT EVs proteomes). Interestingly, proteins that are usually present in mitochondria (e.g., cytochrome c oxidase subunit 5A (Cox5a), ATP synthase peripheral stalk subunit OSCP (Atp5o), and superoxide dismutase 2 (Sod2)) were enriched in EVs of the diabetic group. Several of the mitochondrial proteins could be linked to lipid metabolic processes, such as fatty acid break-down (Figure 5F) (e.g., acetyl-CoA acetyltransferase 1 (Acat1), acyl-CoA dehydrogenase medium chain (Acadm), and 2,4-dienoyl-CoA reductase 1 (Decr1)), supporting the observation that altered lipid metabolism in diabetes patients contributes to disease pathology.[50] While the function of those EVs in diabetic wounds remains to be determined, EVs were recently reported to transfer mitochondrial particles.[48a,51] The role of this mitochondrial

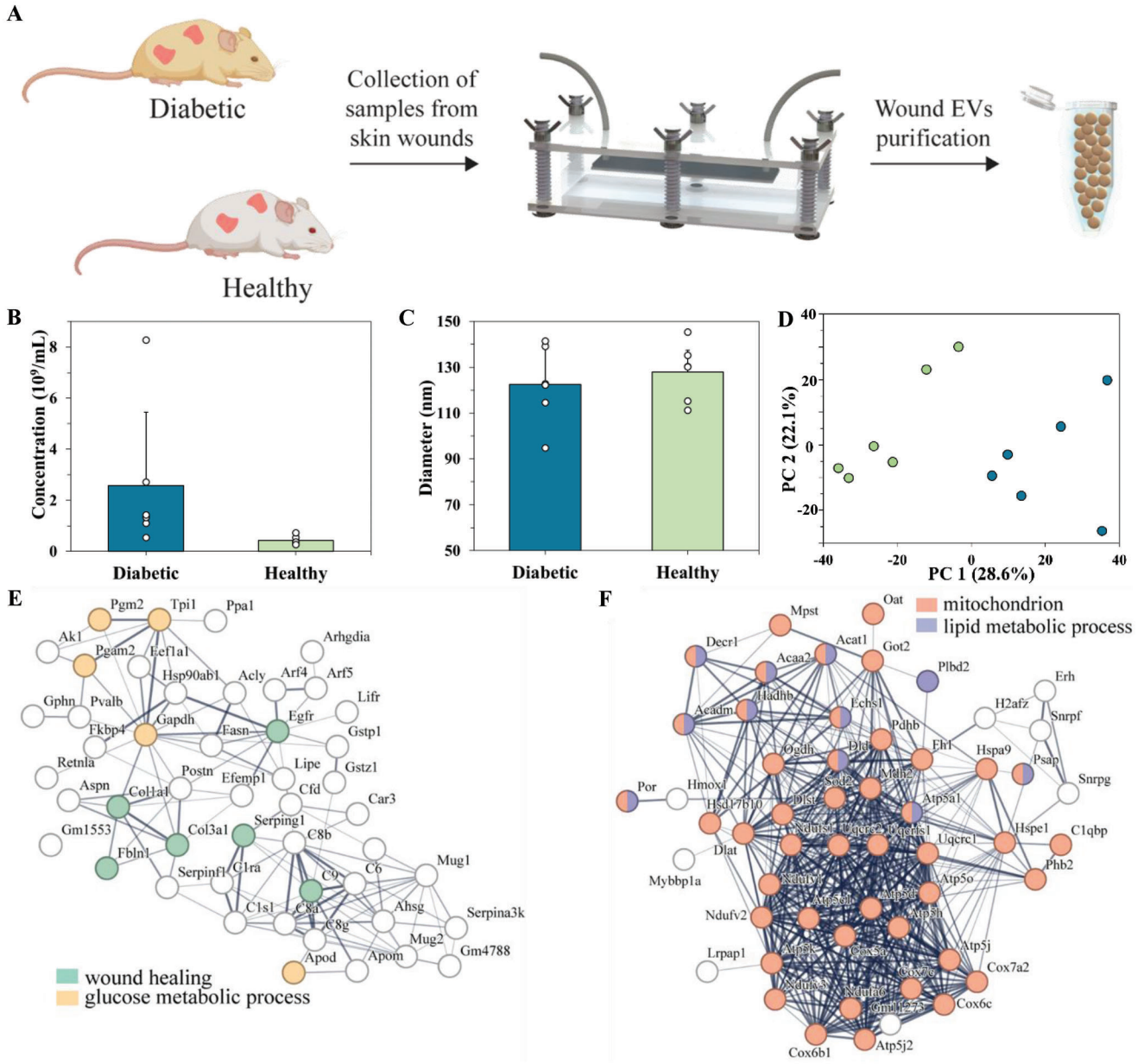

Figure 5. EVs separated from wounds of diabetic versus healthy mice. A) Schematic representation of the experiment. B,C) Summary of NTA analysis of EVs concentration (mean + SD, $n = 6$), $p = 0.129$ (B) and size (mean + SD, $n = 6$) (C) in wound incubation media. D) Principal component analysis of $\log_2$ transformed DIA-derived protein abundances ($n = 6$ samples per group). The eigenvalues of PC1 and PC2 are 635.6 and 489.91, respectively. E,F) STRING protein interaction networks of proteins that were identified as significantly enriched in EVs from WT mouse wounds (glucose metabolism, wound healing) (E) and EVs from diabetic mouse wounds (mitochondrion, lipid metabolism) (F). Nodes indicate proteins, edges indicate interactions, and the thickness of edges indicates the strength of data support.[53]

transfer mechanism was found to depend on the nature of the secreting as well as the receiving cells. In some pathologies, cells with impaired mitophagy export damaged mitochondrial particles via EVs.[51a] Although speculative as we did not assess mitochondrial function, the increase in mitochondrial proteins in the EVs from diabetic wounds points an attempt to remove damaged mitochondria, potentially due to reduced mitophagy capacity.[52] Consistent with our findings in mouse skin wounds, damaged mitochondrial particles were enriched in circulating EVs of obese patients originating from stressed adipocytes, but not in those of a lean cohort.[48a] Our data also showed that EVs from WT mice included more proteins linked to wound healing and glucose metabolic processes (e.g., epidermal growth factor receptor (Egfr), fibulin 1 (Fbln1), and glyceraldehyde-3-phosphate dehydrogenase (Gapdh)) (Figure 5E) compared to EVs from diabetic mice. These results suggest that EVs secreted from wounds of diabetic mice may fail to transfer signals that promote wound healing, and rather mediate diabetes-related stress signals.

2.6. EVs Separation and Subsequential Loading Using Our "All-In-One" Microstructured Electrochemical Fluidic Device

Finally, we investigated whether the device can be used to improve loading protocols with polyplexes, displaying an additional feature of an integrative system toward therapeutic applications. It was previously published that EVs can be loaded with siRNAs following incubation with poly(ethyleneimine) (PEI):siRNA complexes.[54] Therefore, we determined whether the EVs can be isolated, loaded with a model siRNA, and purified from excess polymer, with a single device. Human urine was injected into the fluidic channel that was pre-modified with the anti-CD9 antibody. Following the EVs' attachment, the PEI:siRNA complex was introduced into the device. Excess PEI:siRNA was washed from the channel prior to the electrochemical release (**Figure 6**A). The removed PEI was quantified by fluorescence analysis using fluorescein isothiocyanate (FITC)-labeled PEI. Approximately 65% and 70% of the PEI were flushed away with 1 or 3 mL of the washing buffer, respectively (Figure S8A, Supporting Information). The median diameter of the released EV-PEI:GFP siRNA complex was 118 ± 18 nm (Figure S8B,D, Supporting Information). TEM image of loaded EVs demonstrated the morphology change upon complex formation (Figure 6B). Pre-separated EVs that were manually mixed with PEI:GFP siRNA[54] (and not treated with the device) had a larger median size of 219 ± 9 nm, and a higher number of detectable particles (Figure S8B–D, Supporting Information), while the PEI:siRNA complexes were not detected by NTA. A control experiment with a non-modified device (no capturing antibodies) subjected to a similar complex preparation process did not yield detectable particles. The zeta potential value of the EVs manually mixed with PEI:GFP siRNA was +36.8 ± 2.3 mV, whereas bare EVs had a typical zeta potential of −28.2 ± 5.2 mV. The removal of excess PEI:GFP siRNA through the device reduced the positive charge to +4.1 ± 2.4 mV (Figure 6C). Furthermore, increasing the concentration of the loading solution for complex preparation with the device by 5 and 10 folds resulted in particles having zeta potentials of ca. +35 and +40 mV, respectively (Figure S8E, Supporting Information), making those modified EVs potentially more toxic. While colloids with highly positive zeta potentials resulting from the assembly of excess cationic polymers with siRNA may be taken up by cells to a greater extent, they are also often associated with toxicity and are prone to aggregate in physiological media.[55] Hybridizing EVs with a PEI:siRNA prepared with labeled siRNA conjugated with Cy5, resulted in vesicles with similar sizes but more positive charges (+30 to +50 mV) (Figure S8F–I, Supporting Information), which might be explained by changes in the macromolecular complex rearrangement.[56] Electrophoretic mobility shift assay showed that both types of complexes (mixed manually or via the device) completely inhibited the migration of the free siRNA toward the positive electrode (Figure 6D). We further evaluated the cellular uptake of Cy5-labeled siRNA-loaded EVs (Figure 6E,F). Similarly to manually prepared EV-PEI:siRNA complexes, those prepared via the device were taken up by HeLa-GFP cells, although the approximate amount of PEI:siRNA in the device-prepared complexes was lower in comparison with the manually prepared one. Furthermore, stability evaluation of this complex in 95% serum revealed a gradual release of the Cy5-siRNA within 36 h of incubation as shown by the increased intensity of the free Cy5-siRNA band (Figure S9, Supporting Information). Altogether, these data suggest that EVs were manipulated with exogenous siRNA subsequently to their purification using our "all-in-one" platform. Excess wash resulted in a reduced charge of the solution, demonstrating the advantages of this preparation method compared with conventional approaches for downstream therapeutic applications.

3. Conclusion

A simple electrochemical device was used to rapidly isolate EVs directly from different physiological fluids. A unique combination between PDMS, which conventionally serves as a platform for microfluidics fabrication, and the micro-carbon fibers, which are traditionally used as air-permeable electrodes, formed a novel composite material. This integration enabled, on the one hand, the formation of a confined fluidic channel for efficiently flowing a raw bio-sample, and on the other hand, the selective capture of an analyte in large quantities and its controlled release. The device was manufactured from inexpensive materials in a robust fashion. The fabrication is based on aluminum molds and does not require a clean-room facility, allowing easy scalability of the process. Phase gas modification of the electrodes' surface can be performed simultaneously on several devices, using low quantities of the chemical reagent, without the need for organic solvents. In comparison with other emerging microfluidic-based methods for EVs isolation, the device can be manufactured at a low cost. The inherent use of a reference electrode enables to perform quality control for the reproducibility of the device performance and may be applied for simultaneous sensing in future applications. Due to its low power consumption, the device could in the future be supplied with a battery, rendering it highly portable towards field conditions or patients' bedside applications. Furthermore, simple handling, versatility in terms of sample types and volumes, and rapidness of the purification process may be beneficial factors for application in the medical field. Another important factor is the ability to select the release medium, which means that the obtained solution could be used directly for therapeutic purposes, without further cleaning procedures or buffer exchange. Since EVs capturing is achieved by immunoaffinity, selective isolation of different subpopulations of EVs could, in principle, be easily performed for more in-depth vesicle characterization and diagnostic use, as suggested by the wound EVs data. Compared to other affinity-based microfluidic devices, the use of fibrous material for antibody attachment largely increases the capture capacity. Furthermore, differently from other electrokinetic approaches, the application of an external force for EVs capturing is not required, enabling higher flow rates, channel dimensions, and sample volumes. Finally, specific binding and control over the release step provide the option to introduce loading steps, which were illustrated in this work with polyplexes. Taken together, this device overcomes many of the limitations associated with microfluidics and other emerging EVs' isolation technologies, allowing high throughput and integration with downstream applications. It could therefore meet current needs, and is likely to contribute to advancing the state of the EVs-based research field.

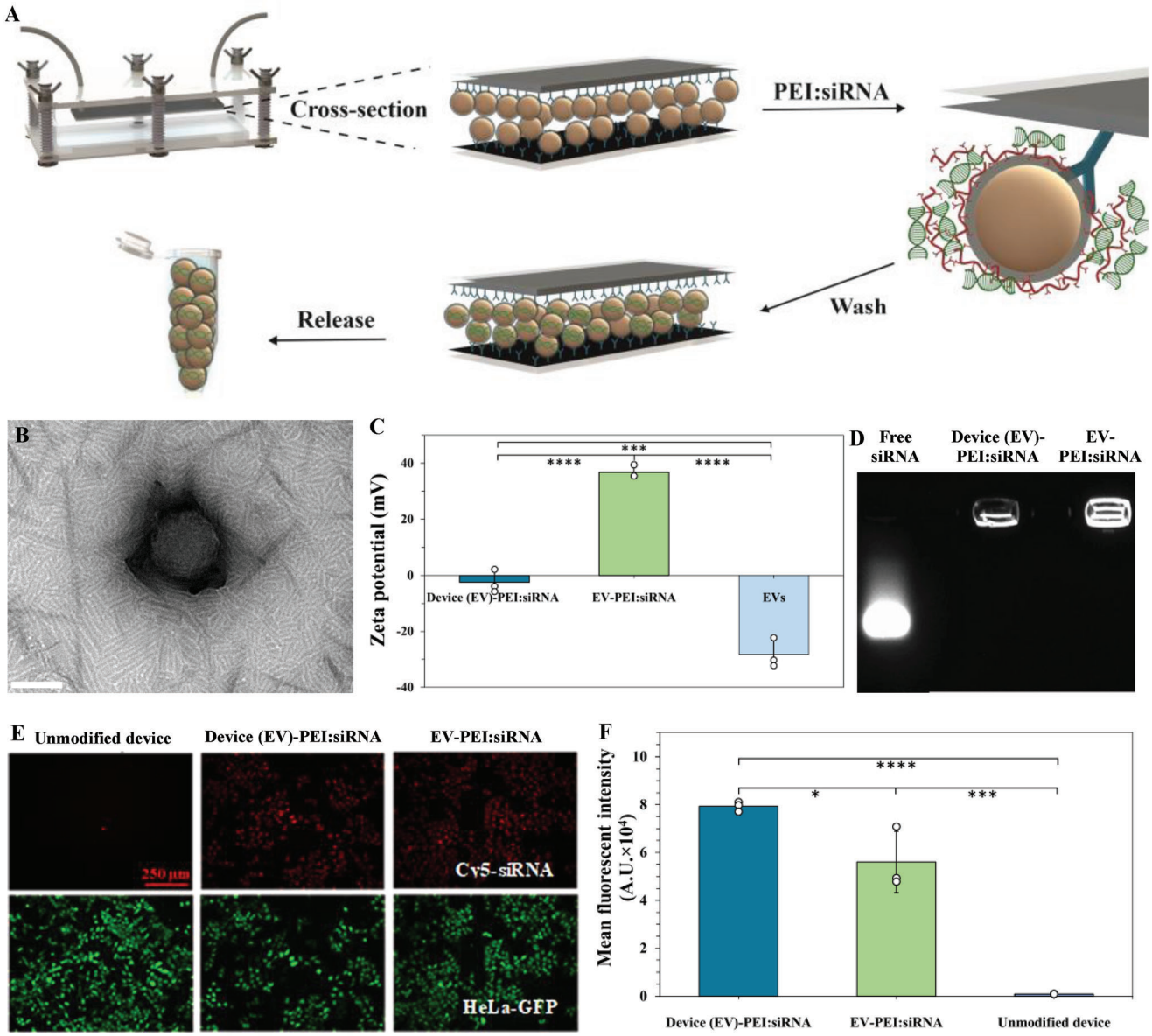

Figure 6. "All-in-one" system for the separation and subsequent loading of EVs. A) Image of the settings used for loading the EVs. B) TEM image of a single EV modified with PEI:GFP siRNA with the device. Scale bar: 100 nm. C) Zeta potential values of the complexes of EVs with PEI:GFP-siRNA prepared via the device (Device (EV)-PEI:siRNA) or manually (EV-PEI:siRNA), mean ± SD ($n = 3$), ****$p = 0.00006$ Device (EV)-PEI:siRNA vs EV-PEI:siRNA, ***$p = 0.0006$ Device (EV)-PEI:siRNA vs EVs, ****$p = 0.000003$ EV-PEI:siRNA vs EVs. D) Electrophoretic mobility shift assay comparing free siRNA with loaded EVs prepared via the device (Device (EV)-PEI:siRNA), or by manual preparation (EV-PEI:siRNA). E). Fluorescence microscopy images demonstrating that both EV-PEI:siRNA-Cy5 complexes prepared with the device (Device (EV)-PEI:siRNA) and the manually mixed EV-PEI:siRNA-Cy5 complexes (EV-PEI:siRNA) were taken up by HeLa-GFP cells, while cells treated with a similar volume of a solution collected from the control experiment (unmodified device) were Cy5 negative. F) FACS assessment of complex internalization to cells. Quantification of the internalization of EVs:PEI:Cy5-siRNA complexes prepared manually or including the device washing step, mean ± SD ($n = 3$), *$p = 0.02$ Device (EV)-PEI:siRNA vs EV-PEI:siRNA, ****$p = 0.00003$ Device (EV)-PEI:siRNA vs unmodified device, ***$p = 0.0003$ EV-PEI:siRNA vs unmodified device.

4. Experimental Section

Materials: 3-Aminopropyldimethylethoxy-silane (S00750-5 g) and fluorescein isothiocyanate (471600-1 g) were purchased from Fluorochem. Mouse monoclonal IgG1 κ CD9 antibody (C-4) (sc-13118), mouse monoclonal IgG1 κ CD63 antibody (MX-49.129.5) (sc-5275), and mouse monoclonal IgG1 κ CD9 (C-4) Alexa Fluor 647 (sc-13118) were purchased from Santa Cruz. Dulbecco's modified Eagle medium (DMEM) high glucose, GlutaMAX supplement, fetal bovine serum (FBS), and phosphate-buffered saline (PBS), were purchased from Gibco. Penicillin and streptomycin were purchased from Thermo Fisher Scientific. Silver/silver chloride paste (60/40), skim milk powder, potassium chloride (KCl), (4-(2-hydroxyethyl)-1-piperazineethanesulfonic acid) (HEPES), Tris, polysorbate 20, and ethanol (ethanol absolute >99.8% for analysis, 100983 1000–1lt), were purchased from Sigma–Aldrich. Glycerol was purchased from VWR chemicals. SYLGARD 184 silicon elastomeric kit was purchased from Dow

Corning. Linagliptin was purchased from Cayman Chemical Company. Malachite green was purchased from Bender & Hobein GmbH. Ammonium molybdate tetrahydrate was purchased from abcr GmbH. GFP siRNA (5′-GAA CUU CAG GGU CAG CUU GGG −3′, M_w = 13 365.1 g mol^{-1}) was purchased from Mycrosinth. Cy5-conjugated negative control #2 siRNA (M_w = 13 836 g mol^{-1}) was purchased from Sigma–Aldrich (SIC006-5×1NMOL). Poly(ethylenimine) (PEI, branched average $M_n \approx 10\,000$) was purchased from Sigma–Aldrich (408727-100ML). DIW was supplied by a Merck Millipore MilliQ Direct-Q8. The source of other chemicals is mentioned in the latter sections. All the chemicals were used as received without further purification.

Fabrication of the Fluidic Device: The device was composed of a 3D carbon electrode bearing a high surface area embedded in a PDMS-based microchannel. The µCF electrode was made of Freudenberg H23 (22 cm × 30 cm, catalog (cat) number: 1590042) carbon paper (Freudenberg Performance Materials SE & Co. KG). For a 58-mm long fluidic channel, the WE, CE, and RE had areas of 4.64, 4.24, and 0.24 cm^2, respectively. The fluidic channel was integrated with silicon tubing, which allowed the flow of the biosamples, injected with the help of syringes.

The first step of the device assembly is the fabrication of the microchannels. For this, two molds, previously washed with ethanol, were used. Then, double-sided adhesive carbon tape (8 mm × 20 m, cat AGG3939, Agar Scientific Ltd.), was taped on the molds. µCF electrodes (Freudenberg H23, 22 cm × 30 cm, 0.15 mm thickness, cat. 1590042, Freudenberg Performance Materials SE & Co. KG) were positioned on top of the tape. On the reference electrode, Ag/AgCl (60/40%m/m, 901773-50G, Sigma-Aldrich) paste was applied to form a thin 3–4 mm layer, then dried in the oven at 80 °C. Afterward, silicon tubes (1 mm inner diameter, 3 mm outer diameter, 4.5 cm length, Millipore), were inserted into the counter electrode with the help of needles (100 Sterican ø 0.90 × 50 mm, 20 G×2″, Braun Injekt; Figure S1B, Supporting Information). Then, PDMS (50 g) and a curing agent (5 g) were mixed. The resulting whitish mixture was poured onto the molds, whose sides were delimited by microscope slides (26 × 76 × 1 mm Menzel X50, Thermo Fisher Scientific) covered in aluminum foil. The PDMS curing occurred at 80 °C for 1 h (Figure S1C, Supporting Information). The two semi-channels were then carefully removed. The electrodes were thoroughly washed with ethanol and then with DIW. The resistance of the electrodes and the quality of the contacts were measured using a Digital Multimeter (UNI-T UT61E, Unitrend Technology). The conductivity of the WE and CE was tested to be ≈3 Ω cm^{-1}.

Functionalization of the µCF Electrodes: The two semi-channels with the embedded µCF electrodes were washed with 40 mL of ethanol and dried in a vacuum oven (100° C, 30 min under vacuum). Then, an RF source at 60 W for 1 min, at an oxygen gas pressure of 30 Pa, (CY-P2L-B150, Zhengzhou CY Scientific Instrument Co.) was initiated, to induce the formation of hydroxyl groups. Silanization was then performed by a gas phase chemical adsorption of APDMES (300 µL), for 16 h at 100 °C and 0 Pa in a covered glass Petri dish, followed by heating to 105 °C under vacuum for 2 h. The semi-channels were washed with 50 mL of ethanol and dried under vacuum at 100 °C, using a vacuum oven (KVTS11, Salvis, AG. Emmenbrücke).

Fluidic Electrochemical Controlled Channel Assembly and Characterization: The two semi-channels were adjusted together to form a fluidic channel, and tightened between two clear poly(methyl methacrylate) (PMMA) lids (105 mm × 55 mm × 5 mm), using six bolts and six nuts. Steel needles were inserted into the PDMS, in a manner that penetrates through the µCF electrodes, without contacting the fluidic channel and the tubing. The fluidic system was then washed with 5 mL of DIW and with 5 mL of PBS. The metal needles were connected to a potentiostat (EmStat3 Blue, PalmSens BV). The electrochemical cell, inside the fluidic channel, was characterized by cyclic voltammetry, using PBS buffer, and the following conditions: scan rate = 0.02 V s^{-1}, step = 0.002 V, E_{begin} = 0.0 V, $E_{vertex1}$ = 0.1 V, $E_{vertex2}$ = −0.1 V. Anti-CD63, anti-CD73, or anti-CD9 antibodies were immobilized on the electrodes surface, by injecting 300 µL of antibody solution (21.3µg mL^{-1} in PBS) into the fluidic channel, using a 1-mL syringe. On the other end of the fluidic channel, another empty syringe of 1 mL was used to collect the solution. The antibody solution was incubated for 1 h in total at RT, during which the solution was transferred five times between the two syringes every 10 min. After that, 15 mL of PBS (at a flow rate of 0.3 mL s^{-1}) was injected through the channel in order to clean the channel from unadsorbed antibodies.

Quantification of Unadsorbed, Washed, and Released Antibodies: Quantification of unadsorbed washed and released antibodies was performed using Alexa Fluor 647-conjugated anti-CD9 antibody solution (21.3 µg mL^{-1} in PBS, sc-13118 AF647, Santa Cruz Biotechnology). Fluorescence was measured at an excitation wavelength of 645 nm and emission of 675 nm, using an Infinite M200 plate reader (TECAN).

Quantification of Unadsorbed, Washed, and Released Antibodies—Quantification of Unadsorbed Antibodies: Following device assembly, 300 µL of antibody solution was injected into the fluidic channel, using a 1 mL syringe. On the other end of the fluidic channel, another empty syringe of 1 mL was used to push the antibody solution back and forth for maximum attachment. The antibody solution was collected from the syringe at various time points for fluorescence intensity measurement, then injected back into the channel.

Quantification of Unadsorbed, Washed, and Released Antibodies—Quantification of Washed Antibodies: 300 µL of antibody solution were injected into the fluidic channel for antibody coating, using a 1 mL syringe. On the other end of the fluidic channel, another empty syringe of 1 mL was used to collect the solution. The antibody solution was transferred between the two syringes five times every 10 min over a course of 1 h in total. Then, PBS was injected through the channel at a flow rate of 0.3 mL s^{-1}. The solution was collected from the other syringe for fluorescence intensity measurements.

Quantification of Unadsorbed, Washed, and Released Antibodies—Quantification of Released Antibodies: The electrodes' surface was coated with antibodies, as detailed in the section "Fluidic Electrochemical Controlled Channel Assembly and Characterization". 300 µL of DIW were injected into the channel, and voltage was applied. Decreasing potentials were applied (between 0 to −1.8 V) on the WE, and at each point, the solution was collected following voltage application for fluorescence intensity measurement and then injected back into the channel.

Isolation of EVs from Biosamples using the Electrochemical Device—Isolation from Biosamples: All human biosamples were provided by certified commercial providers. Plasma (Single Donor Human Plasma (Blood Derived), IPLASK2E10ML, Innovative Research), was shipped and stored at −79 °C. Serum (Pooled Human Serum Off The Clot, ISER10ML, Innovative Research), was shipped and stored at −79 °C. Plasma and serum samples were collected under ISO, FDA, USDA, and EPA certificates. Urine (Human Urine Male, BioIVT), collected under ISO and FDA certificates, was shipped and stored at −79 °C. 50 mL of HeLa-GFP cell culture medium/urine, and 10 mL of plasma/serum, were injected into the fluidic channel at a rate of 0.3 or 1 mL s^{-1} for the 10 or 50 mL samples, respectively, and pushed back and forth 10 times. The remaining solution was withdrawn from the device and 20 mL of PBS were injected at a rate of 0.3 mL s^{-1} to remove contaminants. Then, for release in DIW, 1 mL of DIW were injected into the device and withdrawn. Before the electrochemical release, a syringe of 1 mL with 1 mL of PBS or DIW was connected to one end of the device, and another empty 1 mL syringe was connected to the second end of the device. Then, the needles of the device were connected to the potentiostat, and a potential of −1.5 V was applied on the working electrode for 45 s, during which the solution was pushed back and forth through the channel. This process was then repeated after interchanging the poles of the electrical cycle.

The estimated repulsive energy that is generated by applying −1.5 V on the electrodes in the presence of DIW is 1.5 × 10^{-19} J according to Equation (1).

$$E\,(\text{repulsive}) = dV \times q \tag{1}$$

where dV is the potential applied on a layer of 100 nm (EVs diameter) from the electrode's surface, When the gap between the electrodes is 200 µm, (dV = −0.75 mV), and q is the total charge of the EVs, according to Equation (2).

$$q = A \times \sigma \tag{2}$$

where σ is the EVs' surface charge density ($\sigma = -6.2$ mC/m^2, $r = 50$ nm), and A is the surface area of the EV according to Equation (3).[57]

$$A = 4\pi r^2 \tag{3}$$

This repulsive energy is ≈2 times larger than the energy of the complex between the antibody and antigen, which is estimated to be -8.5×10^{-20} J, according to Equation (4).

$$E_{(\text{eq, Ab–Ag})} = \frac{R}{N_A} \times T \times \ln(K_d) \tag{4}$$

where R is the gas constant, N_A is the Avogadro constant, and a typical dissociation constant (K_d) for a murine antibody with its antigen is ≈10^{-9} M at RT.[58]

In addition, due to local pH changes near the electrodes upon voltage application, the affinity interactions between the antibodies and the EVs become weaker, and lower energy is required in order to overcome them.[29a]

Afterward, the solution containing the purified EVs in DIW or PBS was withdrawn into the collecting syringe.

Isolation of EVs from Biosamples using the Electrochemical Device—Quantification of Captured EVs Versus the Quantity of Bound Antibody: 300 µL of anti-CD9 solution containing either 0.64, 6.4, or 64 µg were injected into the fluidic channel for antibody coating, as detailed in the section entitled "Fluidic Electrochemical Controlled Channel Assembly and Characterization". EVs were separated from the cell-culture medium as described in the section entitled "Isolation of EVs from Biosamples using the Electrochemical Device". The concentration of the released EVs was measured by NTA as in the section entitled "Characterization of the Isolated EVs—NTA".

Isolation of EVs from Biosamples using the Electrochemical Device—Optimization of Captured EVs Versus the Number of Back-and-Forth Passages: EVs were isolated from the cell culture medium as detailed above (Section "Isolation of EVs from Biosamples using the Electrochemical Device") using the anti-CD9 modified device. The biological samples were injected into the fluidic channel and pushed back and forth for 1, 5, or 10 times, using a Fusion 101 Digital Dual Syringe Pump (Chemyx), within a constant time course of 10 min, by adjusting the flow rate. The concentration of the released EVs was measured by NTA as described in the section entitled "Characterization of the Isolated EVs—NTA".

Isolation of EVs from Biosamples using the Electrochemical Device—Optimization of Captured EVs Versus the Applied Potential: EVs were isolated from the cell culture medium as detailed above (Section "Isolation of EVs from Biosamples using the Electrochemical Device") using the anti-CD9 modified device. EVs were released by applying 0, −0.4, −0.8, −1.2, or −1.6 V. The concentration of the released EVs was measured by NTA as detailed in the section entitled "Characterization of the Isolated EVs—NTA".

Isolation of EVs from Biosamples using the Electrochemical Device—EVs' Capturing Efficiency: EVs pre-separated by UC followed by SEC (qEV10 Gen 2 Columns (70 nm), Izon Science) were spiked into 1 mL PBS in quantities of 4.9×10^{10}, 1.37×10^{11}, and 7×10^{11} particles mL^{-1}. These solutions were injected into the device and subjected to EVs attachment as detailed above (Section "Isolation of EVs from Biosamples using the Electrochemical Device"). The concentration of the EVs withdrawn from the channel without applying release potential was measured by NTA as described in the section entitled "Characterization of the Isolated EVs—NTA". The captured amount was calculated from the initial amount and the unbound EVs.

Isolation of EVs from Biosamples using the Electrochemical Device—EVs' Recovery Rate: EVs pre-separated by UC followed by SEC (qEV10 Gen 2 Columns (70 nm), Izon Science) were spiked into 1 mL PBS. The spiked solutions were injected into the device and subjected to EVs attachment as detailed above (Section "Isolation of EVs from Biosamples using the Electrochemical Device"). The concentration of the EVs withdrawn from the channel following the application of a release potential versus the volume of the release solution was measured by NTA as described in the section entitled "Characterization of the Isolated EVs—NTA".

SERS: 150 µL of Au nanorods solution (40 nm, 5 mg mL^{-1}) were drop castd over 1 cm^2 samples (functionalized and non-functionalized microcarbon fibers surface) and allowed to dry at RT. Raman and SERS spectra were recorded using a confocal Raman microscope (Horiba Raman microscope, LabRAM HR Evolution) with a 325 nm laser source of a maximum power of 300 mW. The measurements were performed with a 40× objective in the Raman microscope with 5% of laser power. The spectral positions were calibrated by the characteristic Si phonon peak at 520.7 cm^{-1}.

SEM–EDX-Spectroscopy: For sample preparation, a full device was cut to show the cross-section and taped on carbon tape on the SEM substrate. SEM and EDX were carried out on a Quanta 200F field-emission-gun scanning electron microscope (FEI). EDX map of the semi-channel cross-section was collected with an acceleration voltage of 20 kV, a sample tilt of 0°, and a working distance of 10 mm. Data were post-processed using chemical indexing with the TEAM WDS software by EDAX.

PEI FITC Labeling: PEI was labeled with FITC in a molar ratio of 1:1 (1 labeled amine group per polymer), by an amine–isothiocyanate conjugation.[59] PEI (770 mg, 0.077 mol) was dissolved in 30 mL of ultrapure water, and mixed with 30 mg (0.077 mmol) of FITC-isothiocyanate. The pH of the solution was adjusted to 11.0 with 0.01 M NaOH solution. The mixture reacted overnight at RT, protected from light. The resulting FITC-labeled PEI (PEI-FITC) was purified against 5 L of DIW for 3 days by dialysis (Spectra/Por 3 Dialysis Membranes, MWCO 3500, Spectrum Laboratories), until no fluorescence was detected in the dialysate, under excitation at 494 nm, and no free FITC was detected in the product by thin layer chromatography (TLC, TLC Silica gel 60 F_{254}, Sigma–Aldrich).

Cell Culture: HS-5 cells were obtained from the American Type Culture Collection (ATCC). HeLa-GFP cells were obtained from Cell Biolabs, Inc. Cells were cultured in DMEM supplemented with 10% FBS, 100 U mL^{-1} penicillin, and 100 µg mL^{-1} streptomycin (full medium), at 37 °C and 5% CO_2. Cells were cultured in tissue culture flasks (75 cm^2) and split twice a week. They were routinely tested for mycoplasma using the MycoAlert Mycoplasma Detection kit (Lonza Group AG) according to the manufacturer's protocol. Passages 1–15 were used for isolation experiments for HS-5 cells, and 10–35 for HeLa-GFP cells. For EVs isolation experiments, cells were seeded in a T300 flask (3.5×10^6 HeLA-GFP cells or 8×10^6 HS-5 cells) in 50 mL of DMEM supplemented with 10% FBS, 100 U mL^{-1} penicillin, and 100 µg mL^{-1} streptomycin. After 48 h, cells were washed twice with 5 mL PBS and 50 mL of FBS-free DMEM were added. The cells were incubated for 48 h at 37 °C and 5% CO_2, then cell culture medium was collected.

Cell Culture—Purification by Ultracentrifugation: The medium was centrifuged sequentially, at 2000*g* for 30 min and at 12 000*g* for 45 min at 4 °C using a Sorvall RC 6 PLUS centrifuge equipped with an SA-600 Fixed Angle Rotor (Thermo Fisher Scientific). For the HS-5-derived EVs, the supernatant was filtered through a 0.22 µm pore-sized filter. Then, the culture media was centrifuged at 110 000*g* and 4 °C for 70 min using an Optima XE-90 ultracentrifuge equipped with a Type 45 Ti Fixed-Angle Titanium Rotor (Beckman Coulter Life Science). The resulting pellets were resuspended in PBS, pooled, and subjected to a second ultracentrifugation under the same conditions.

Cell Culture—CD73 Enzymatic Activity Assay: The CD73 activity of EVs was measured following previous protocols.[38] Briefly, EVs samples were prepared by incubating 0.1 µg of EVs protein, as measured by the microBCA assay (Thermo Fisher Scientific) according to the manufacturer's protocol, with 30 µL (800 µM) AMP solution in 60 µL of 10 mM TRIS buffer pH 7.4. The plate was incubated for 10 min at RT before the enzymatic reaction was stopped by adding 40 µL color reagent (0.034% w/v malachite green (Bender & Hobein GmbH), 1.55% w/v ammonium molybdate tetrahydrate (abcr GmbH), and 0.0625% v/v polysorbate 20) into each well, (V_{final} = 100 µL). The plate was incubated for 1 h at RT and the absorbance was measured at 620 nm using an Infinite M200 plate reader (TECAN).

Characterization of the Isolated EVs—NTA: NTA was performed on a PMX 120 ZetaView Mono Laser device (Particle Metrix GmbH), equipped with a 405 nm laser and a CMOS camera. Data analysis was performed

on the ZetaView software version 8.04.04 SP2, applying a bin class width of 5 nm, a minimum brightness of 25, a minimum area of 5, a maximum area of 1000, and a trace length of 15. The device was first calibrated with polystyrene beads (MFCD00131491, Sigma-Aldrich) diluted by 1:500 000 (v/v) at a concentration of ≈100 particles per frame. For the measurements, the shutter was set to 150, the sensitivity to 85, and the frame rate to 30. EVs samples were diluted 1:50 (v/v) in DIW for the measurements. Each measurement was performed in triplicate. All data were smoothed by moving average trendline (period = 4). Zeta potential measurements were performed with a pulse mode, using similar settings as detailed above.

Characterization of the Isolated EVs—TEM: 300-mesh copper grids with ultrathin carbon support film were negatively glow-discharged in a PELCO easiGlow discharge cleaning system (Ted Pella Inc.) at 25 mA for 30 s at a pressure of 38 Pa. Then, 4 µL of EVs solution were absorbed for 30 s onto the grids and the grids were treated with uranyl acetate or phosphotungstic acid staining solution and washed with DIW. After removing excess liquid with filter paper, the grids were dried under ambient conditions. The samples were imaged with a Tecnai F20 field-emission-gun microscope (FEI) equipped with a combination of a CCD camera (ORIUS SC200 2K) and a direct electron detector (Falcon II 4K) at an acceleration voltage of 120 kV. The microscopy images were acquired in the bright field mode.

Characterization of the Isolated EVs—Cryo-TEM: For cryo-TEM imaging, samples were directly applied onto an EM grid, vitrified, and visualized. The vitrobot system was used as the specimen preparation unit. This semi-automated plunging device with humidity and temperature control was used to form vitreous ice by rapid cooling of a thin layer of aqueous sample in ethane. Before cooling, 3.4 µL of the sample were blotted on a lacey-carbon supported Cu grid, 300 mesh. The waiting time for the sample on the grid was 10 s. In order to obtain a good ice thickness, the blotting time was set to 2.5 s, the blotting force to 0, and the temperature to 22 °C.

The cryo-EM images were acquired at Titan Krios FEG (Thermo Fisher Scientific) at 300 kV using a direct electron detector (Falcon III 4k × 4k) (Thermo Fisher Scientific), which works in tandem with a Ceta 16 M 4k × 4k CMOS detector (Thermo Fisher Scientific) and K2 (Gatan) with the Quantum LS energy filter (Gatan).

Characterization of the Isolated EVs—SEM: The EVs-containing solution in DIW was dropped on a Freudenberg H23 carbon paper (Freudenberg Performance Materials SE & Co. KG) and allowed to dry. Images were taken using Quanta 200 environmental SEM (FEI) at high vacuum, 10 kV, and secondary-electrons detector.

Characterization of the Isolated EVs—Western Blot Analysis: Samples of isolated EVs (≈1 mL) were lyophilized and resuspended in 30 µL of DIW. Eight µg urinary EVs, 8 µg serum EVs, and 3 µg EVs from HS-5 culture medium, as measured by the microBCA assay (Thermo Fisher Scientific) according to the manufacturer's protocol, were added with 5:1 (v/v) sample buffer (Tris HCl 1 M, 10% (w/v) SDS, 30% (v/v) glycerol, 0.02% (w/v) bromophenol blue, pH 6.8), and heated for 5 min at 95 °C. Then, samples were loaded on a 12% polyacrylamide gel and run at 90–100 V in a running buffer (3% (w/v) Tris base, 14.4% (w/v) glycine, and 1% (w/v) SDS). Proteins were transferred to 0.2 µm pore-sized Immun-Blot PVDF membranes (Bio-Rad Laboratories Inc.) using the Trans-Blot Turbo Transfer system for 10 min, at 17 V and 1.3 A. The membranes were then blocked with 5% (w/v) skim milk in Tris-buffered saline (TBST, 20 mM Tris, 150 mM NaCl, 1% v/v polysorbate 20) for 1 h at RT. Then, the membrane was incubated with antibodies: mouse monoclonal anti-CD9 antibody (sc-13118), mouse monoclonal anti-CD63 antibody (sc-5275), mouse monoclonal anti-TSG101 antibody (sc-7964), and mouse monoclonal anti albumin antibody (sc-271605), (all from Santa Cruz Biotechnology), (1:200 v/v in TBST) overnight at 4 °C. After three washes with TBST (10 min, RT), the membrane was incubated with a secondary horseradish peroxidase (HRP)-conjugated polyclonal goat anti-mouse antibody (Dako) (1:2000 v/v in TBST) for 3 h at RT. Then, the membranes were washed three times with TBST (10 min). Membranes were incubated with Western Blotting Luminol reagent (Santa Cruz Biotechnology) according to the manufacturer's protocol and imaged using a ChemiDoc MP Imaging System (Bio-Rad).

Characterization of the Isolated EVs—Nano FCM: EVs samples dissolved in PBS were measured using a NanoAnalyzer N30 instrument (nanoFCM CO Ltd) and analyzed with the nanoFCM Professional Suite software. The instrument was first calibrated with Quality control beads (0.25 µm Fluorescent Silica Microspheres). The sampling pressure was set to 0.8 kPa. Silica nanosphere cocktails (S16M-Exo) were used with a size range between 40 and 200 nm, as size standards. Samples were boosted for 45 s, and the events were recorded for 60 s.

Reusability Assessment: HeLa-GFP cells were seeded in a T300 flask (3.5×10^6 cells) in 50 mL of full DMEM, then cultured for 2, 3, or 4 days. The cells were washed twice with 5 mL PBS and 50 mL of FBS-free DMEM were added. The cells were incubated for 48 h at 37 °C and 5% CO_2, then cell culture medium was collected. EVs were isolated from the medium as detailed in the section entitled "Isolation of EVs from Biosamples using the Electrochemical Device—Isolation from Biosamples".

Three subsequent isolations were performed on each isolation day. First, EVs were isolated from the cells that were cultured for 2 days in full DMEM. Following the isolation of the EVs from the first culture flask, the device was washed with 10 mL of DIW, during which a potential of −1.5 V was applied, and then with 1 mL of PBS. Afterward, the medium from the second culture flask was injected, and EVs were isolated as described above. The same washing procedure was applied, following by the injection of the medium for the third separation. Then, the device was disassembled. The two semi-channels were washed with DIW and ethanol using squeeze bottles. The semi-channels were then placed in a vacuum oven and heated to 100 °C under vacuum for 30 min. Then, the device was stored at RT until the next use. For the next separation, HeLa-GFP cells were cultured in full medium for 3 days. The electrodes of the device were re-activated and modified according to sections "Functionalization of the µCF Electrodes" and "Fluidic Electrochemical Controlled Channel Assembly and Characterization". A similar separation experiment was performed with 3 flasks of culture medium. The process was repeated once again, this time with cells that were cultured for 4 days in full medium.

Animals and Wound Healing Experiments—Wounding and EVs Isolation: Mouse maintenance and animal experiments were approved by the local veterinary authorities (Kantonales Veterinäramt Zurich, Switzerland) (approval numbers ZH016/19 and ZH 015/2022 to S.W.). Four full-thickness excisional wounds (5 mm diameter) were generated using a biopsy punch (Covetrus/Provet AG), on the back skin of anesthetized male C57BL/6JRj (wild type) or BKS(D)-Leprdb/JorlR (diabetic) mice (Janvier Labs, Le Genest-Saint-Isle, France), at the age of 9–10 weeks as previously described.[60] Wounds were allowed to heal without a dressing. Mice were sacrificed at day 7 post-wounding, and the wound was excised using a 5 mm biopsy punch and transferred into a 1 mL PBS-containing tube for EVs isolation, and stored at 4 °C. All four wounds collected from a single mouse were then combined in 5 mL of PBS and incubated at 37 °C, for 10 min, allowing to collect both the EVs from wound exudates and the interstitial fluids. Then, the blinded tubes were vortexed for 3 s, and fluids were injected into a device, pre-functionalized with an anti-CD9 antibody. EVs were released into 1 mL DIW. The released EVs samples were analyzed by NTA, or lyophilized and sent for proteomic analysis.

Animals and Wound Healing Experiments: Proteomic Analysis—EVs Proteome Analysis: Samples were dissolved in 1% sodium deoxycholate in 50 mM ammonium bicarbonate buffer pH 8, reduced with 1 mM dithiothreitol, and alkylated using 5.5 mM iodoacetamide for 10 min at RT. Proteins were in-solution digested with trypsin (Promega). Sodium deoxycholate was precipitated using 50% TFA (trifluoroacetic acid) and tryptic peptides were purified by STAGE tips prior to LC–MS/MS measurements. The latter were performed on a QExactive HF-X mass spectrometer (Thermo Fisher Scientific) coupled to an EasyLC 1000 nanoflow-HPLC (Thermo Fisher Scientific). Peptides were separated on fused silica HPLC-column tip (I.D. 75 µm, New Objective, self-packed with reprosil-Pur 120 C18-AQ, 1.9 µm (Dr. Maisch) to a length of 20 cm), using a gradient of A (0.1% formic acid in water) and B (0.1% formic acid in 80% acetonitrile in water). The mass spectrometer was operated in the data-independent mode. Briefly, after each survey scan (mass range m/z = 350–1200; resolution: 120 000), 28 DIA scans with an isolation width of 31.4 m/z were performed covering a total range of precursors from 350 to 1200 m/z. AGC

target value was set to 3×10^6, a resolution of 30 000, and normalized collision energy to 27%. Data were analyzed using Spectronaut software version 15.7 (Biognosys) with standard settings (without imputation) in direct DIA mode using reference proteome of mus musculus (UniProt, full length) and common contaminants. Further data processing were performed using Perseusm.[61]

Animals and Wound Healing Experiments: Proteomic Analysis—MS Data Quantification and Statistical Analysis: DIA-based LC–MS/MS measurements were obtained for all samples. DIA intensity (called PG quantity) was used for EVs proteome analyses. For EVs content analysis, samples with six valid values in each group were considered, and the DIA intensity values were normalized to the median of each respective replicate. Statistical significance was calculated using a student's *t*-test with false discovery rate (FDR) corrected *p*-values < 0.05. Perseus software (version 1.6.2.3) was used for all the statistical analyses. Gene ontology (GO) analyses were performed for significantly enriched proteins in each group using the STRING database.[62]

Loading Experiments—Preparation of Complexes: 3.7 mg of PEI were dissolved in 4.45 mL of 5% (w/w) glucose solution in DIW, then diluted 1:10 (v/v) in 5% (w/w) glucose solution in DIW. 1 nmol of siRNA was dissolved in 800 µL of 5% (w/w) glucose solution in DIW. The two solutions were mixed at a 1:1 (v/v) ratio and 5:1 PEI:siRNA mass ratio and incubated at RT for 45 min. EVs from 50 mL of urine were separated with the device using the protocol described in the section entitled "Isolation of EVs from Biosamples using the Electrochemical Device—Isolation from Biosamples" with the following modifications: the samples were pushed back and forth through the device 3 times instead of 10 times in order to obtain a smaller amount of EVs. For the manual preparation, EVs released into 1 mL of DIW were added with 300 µL of the PEI:siRNA complex then incubated for 15 min at RT and sonicated for 3 min at RT. For the preparation of the complex via the device, the device was washed with 20 mL of PBS after EVs attachment. At this point, 300 µL of the PEI:siRNA complexes were added and incubated for 15 min at RT. Then, 1 or 3 mL of DIW were injected and withdrawn in order to wash remaining transfection reagent. After that, the complexes were released by the application of −1.5 V.

Quantification of the amount of the released PEI against the washing volume was performed using the FITC-conjugated PEI by measuring the fluorescence of the complex in an Infinite M200 Pro plate reader (Tecan), at excitation wavelength of 490 nm and emission of 525 nm.

Loading Experiments—Cy5-siRNA Internalization Experiment: HeLa-GFP cells were seeded in a 24-well plate at a density of 25 000 cells per well in 1 mL DMEM supplemented with 10% FBS, 100 U mL^{-1} penicillin, and 100 µg mL^{-1} streptomycin. 24 h later, the medium was replaced with 1.5 mL of fresh medium, and cells were treated with 300 µL of EV-PEI:siRNA solution prepared as detailed in the section entitled "Preparation of Complexes", and added with 30 µL of ×10 concentrated PBS solution, at 2.3×10^8 normalized particles number, as determined by the NTA measurements. As a control, 300 µL of the solution were obtained from the device without modification (with 30 µL ×10 concentrated PBS solution). 18 h later, cells were imaged using a DMI6000 fluorescence microscope (Leica Microsystems). Results were quantified using ImageJ software (NIH).

Loading Experiments—Electrophoretic Mobility Shift Assay: 30 µL of samples were supplemented with 5 µL of glycerol 50% solution in DIW (v/v), then loaded on a 1% (w/v) agarose gel in TAE buffer (PanReac AppliChem), and allowed to migrate under 100 V for 15 min. Gels were imaged using a ChemiDoc MP Imaging System (BioRad).

Loading Experiments—Fluorescence-Activated Cell Sorting (FACS)-Based Assessment of Complex Internalization by Cells: HeLa-GFP cells were seeded in a 24-well plate at a density of 12500 cells per well in 0.5 mL DMEM supplemented with 10% FBS, 100 U mL^{-1} penicillin, and 100 µg mL^{-1} streptomycin. 24 h later, the medium was replaced with 0.5 mL of fresh full medium, and cells were treated with 100 µL of EV-PEI:siRNA solution, supplemented with 10 µL ×10 PBS at 40 nM Cy5-siRNA equivalent concentration, as measured by a Tecan Infinite M200 plate reader against Cy5-siRNA calibration curve, using an excitation wavelength of 645 nm and emission of 675 nm. 100 µL of the solution obtained from the device without modification (without particles according to NTA), were supplemented with 10 µL ×10 concentrated PBS solution. After 36 h, the medium was removed, cells were washed twice with PBS, then harvested with 100 µL of trypsin. 400 µL of full DMEM were added, and samples were transferred to Eppendorf tubes and centrifuged (300*g*, 4 °C, 10 min). The medium was decanted, and cells were suspended in 100 µL of FACS buffer (2 mM EDTA, 0.5% BSA in PBS). Samples were analyzed using a Cytoflex 5 instrument (Beckman Coulter).

Loading Experiments—Serum Stability of the EV-PEI:siRNA-Cy5 Complex: Complexes of EV-PEI:siRNA-Cy5 were prepared as detailed above. The complex was kept at 4 °C protected from light, and the first sample of 10 µL was mixed with 190 µL of FBS, and incubated at 37 °C, protected from light. This procedure was repeated at each time point. After 48 h from complex preparation, 30 µL of each sample were supplemented with 5 µL of glycerol 50% solution in DIW (v/v), then loaded on a 1% (w/v) agarose gel in TAE buffer (PanReac AppliChem). The samples were allowed to migrate under 100 V for 30 min. Gels were imaged using a ChemiDoc MP Imaging System (BioRad).

Statistical Analysis: All results are presented as mean ± SD. *p*-Values were calculated using Student's *t*-test with a two-tailed distribution and unequal variance. For comparison of more than two groups, one-way analysis of variance (ANOVA) with post hoc Tukey honestly significant difference (HSD) test was used. $*p < 0.05$, $**p < 0.01$, $***p < 0.001$, $****p < 0.0001$.

Supporting Information

Supporting Information is available from the Wiley Online Library or from the author.

Acknowledgements

This work was supported by the ETH Zurich – Open ETH project SKINTEGRITY.CH, the Swiss National Science Foundation (grant 310030-212212/1 to S.W.), the canton and the University of Fribourg, Switzerland (research grant to J.D.), the Botnar Research Center for Child Health (Postdoctoral Excellence Program support to N.Z.) and BRIDGE, the joint funding programme of the SNSF and Innosuisse (proof-of-concept fellowship to A.K.). The authors thank Miroslav Peter and Stephan Handschin, ScopeM, ETHZ, for support and assistance with TEM and Cryo-EM imaging, Dr. Lee Sung Sik, ETH Zurich, for assistance with the Raman measurement, David Stapfer from the mechanical workshop of the Department of Chemistry and Applied Biosciences of ETH Zurich for fabricating the aluminum molds and the PMMA lids for the device, and Dr. Philipp Schätzle, Cytometry Facility of the University of Zurich (UZH), for support with the operation of NanoFCM. J.D., J.-C.L., and S.W. are members of the SKINTEGRITY.CH collaborative research consortium.

Open access funding provided by Eidgenossische Technische Hochschule Zurich.

Conflict of Interest

V.K., A.K., and J.-C.L. have filed a patent application related to this work.

Data Availability Statement

The data that support the findings of this study are openly available in ETH Zurich research collection at https://doi.org/10.3929/ethz-b-000624031. The mass spectrometry proteomics data have been deposited to the ProteomeXchange Consortium via the PRIDE partner repository, https://proteomecentral.proteomexchange.org/cgi/GetDataset with dataset identifier PXD039342.

Keywords

carbon microfibers, electrochemical devices, exosomes, extracellular vesicles, immunoaffinity, preconcentration, purification

Received: December 21, 2022
Revised: July 4, 2023
Published online: September 19, 2023

[1] a) P. Rodrigues, C. Melim, F. Veiga, A. Figueiras, *Processes* **2020**, *8*, 1561; b) E. Van der Pol, A. N. Böing, P. Harrison, A. Sturk, R. Nieuwland, *Pharmacol. Rev.* **2012**, *64*, 676; c) G. Van Niel, G. d'Angelo, G. Raposo, *Nat. Rev. Mol. Cell Biol.* **2018**, *19*, 213.

[2] a) S. El Andaloussi, I. Mäger, X. O. Breakefield, M. J. Wood, *Nat. Rev. Drug Discovery* **2013**, *12*, 347; b) O. M. Elsharkasy, J. Z. Nordin, D. W. Hagey, O. G. de Jong, R. M. Schiffelers, S. E. Andaloussi, P. Vader, *Adv. Drug Delivery Rev.* **2020**, *159*, 332; c) M. P. Zaborowski, L. Balaj, X. O. Breakefield, C. P. Lai, *Bioscience* **2015**, *65*, 783; d) G. Raposo, W. Stoorvogel, *J. Cell Biol.* **2013**, *200*, 373.

[3] a) B. György, T. G. Szabó, M. Pásztói, Z. Pál, P. Misják, B. Aradi, V. László, E. Pállinger, E. Pap, A. Kittel, *Cell. Mol. Life Sci.* **2011**, *68*, 2667; b) C. Théry, L. Zitvogel, S. Amigorena, *Nat. Rev. Immunol.* **2002**, *2*, 569.

[4] a) Y. Couch, E. I. Buzàs, D. Di Vizio, Y. S. Gho, P. Harrison, A. F. Hill, J. Lötvall, G. Raposo, P. D. Stahl, C. Théry, *J. Extracell. Vesicles* **2021**, *10*, e12144; b) M. Yáñez-Mó, P. R.-M. Siljander, Z. Andreu, A. Bedina Zavec, F. E. Borràs, E. I. Buzas, K. Buzas, E. Casal, F. Cappello, J. Carvalho, *J. Extracell. Vesicles* **2015**, *4*, 27066; c) X.-C. Jiang, J.-Q. Gao, *Int. J. Pharm.* **2017**, *521*, 167.

[5] a) P. Fonseka, A. L. Marzan, S. Mathivanan, in *New Frontiers: Extracellular Vesicles*, Springer, Berlin, Germany **2021**; b) K. G. Ronquist, *Clin. Chim. Acta* **2019**, *488*, 116.

[6] S. R. Iyer, A. L. Scheiber, P. Yarowsky, R. F. Henn, III, S. Otsuru, R. M. Lovering, *Am. J. Sports Med.* **2020**, *48*, 2277.

[7] S. Kourembanas, *Annu. Rev. Physiol.* **2015**, *77*, 13.

[8] Y.-S. Chen, E.-Y. Lin, T.-W. Chiou, H.-J. Harn, *Tzu Chi Med. J.* **2020**, *32*, 113.

[9] M. Lu, E. DiBernardo, E. Parks, H. Fox, S.-Y. Zheng, E. Wayne, *Front. Immunol.* **2021**, *12*, 566299.

[10] R. Moreira, L. S. Mendonça, L. Pereira de Almeida, *Int. J. Mol. Sci.* **2021**, *22*, 12288.

[11] M. Tkach, C. Théry, *Cell* **2016**, *164*, 1226.

[12] a) K. Wu, F. Xing, S.-Y. Wu, K. Watabe, *Biochim. Biophys. Acta, Rev. Cancer* **2017**, *1868*, 538; b) J. McKiernan, M. J. Donovan, E. Margolis, A. Partin, B. Carter, G. Brown, P. Torkler, M. Noerholm, J. Skog, N. Shore, *Eur. Urol.* **2018**, *74*, 731.

[13] a) M. Y. Konoshenko, E. A. Lekchnov, A. V. Vlassov, P. P. Laktionov, *Biomed Res. Int.* **2018**, 2018; b) M. Monguió-Tortajada, C. Gálvez-Montón, A. Bayes-Genis, S. Roura, F. E. Borràs, *Cell. Mol. Life Sci.* **2019**, *76*, 2369; c) L. M. Doyle, M. Z. Wang, *Cells* **2019**, *8*, 727.

[14] M. Eisenstein, *Nat. Methods* **2022**, *19*, 1518.

[15] B. F. Hettich, M. Ben-Yehuda Greenwald, S. Werner, J. C. Leroux, *Adv. Sci.* **2020**, *7*, 2002596.

[16] F. Liu, O. Vermesh, V. Mani, T. J. Ge, S. J. Madsen, A. Sabour, E.-C. Hsu, G. Gowrishankar, M. Kanada, J. V. Jokerst, *ACS Nano* **2017**, *11*, 10712.

[17] K. Sidhom, P. O. Obi, A. Saleem, *Int. J. Mol. Sci.* **2020**, *21*, 6466.

[18] S. Z. Shirejini, F. Inci, *Biotechnol. Adv.* **2021**, 107814.

[19] T. Soares Martins, J. Catita, I. Martins Rosa, O. A. B. da Cruz e Silva, A. G. Henriques, *PLoS One* **2018**, *13*, e0198820.

[20] P. Sharma, S. Ludwig, L. Muller, C. S. Hong, J. M. Kirkwood, S. Ferrone, T. L. Whiteside, *J. Extracell. Vesicles* **2018**, *7*, 1435138.

[21] C. Chen, B.-R. Lin, M.-Y. Hsu, C.-M. Cheng, *J. Vis. Exp.* **2015**, e52722.

[22] E. Multia, C. J. Y. Tear, M. Palviainen, P. Siljander, M.-L. Riekkola, *Anal. Chim. Acta* **2019**, *1091*, 160.

[23] A. Liga, A. Vliegenthart, W. Oosthuyzen, J. Dear, M. Kersaudy-Kerhoas, *Lab Chip* **2015**, *15*, 2388.

[24] E. Reátegui, K. E. van der Vos, C. P. Lai, M. Zeinali, N. A. Atai, B. Aldikacti, F. P. Floyd Jr, A. H. Khankhel, V. Thapar, F. H. Hochberg, *Nat. Commun.* **2018**, *9*, 175.

[25] a) T. Liangsupree, E. Multia, M.-L. Riekkola, *J. Chromatogr.* **2021**, *1636*, 461773; b) M. Morani, T. D. Mai, Z. Krupova, G. van Niel, P. Defrenaix, M. Taverna, *TrAC, Trends Anal. Chem.* **2021**, *135*, 116179; c) J. Chen, P. Li, T. Zhang, Z. Xu, X. Huang, R. Wang, L. Du, *Front. Bioeng. Biotechnol.* **2022**, *9*, 811971.

[26] a) M. Wu, Y. Ouyang, Z. Wang, R. Zhang, P.-H. Huang, C. Chen, H. Li, P. Li, D. Quinn, M. Dao, *Proc. Natl. Acad. Sci. USA* **2017**, *114*, 10584; b) R. T. Davies, J. Kim, S. C. Jang, E.-J. Choi, Y. S. Gho, J. Park, *Lab Chip* **2012**, *12*, 5202.

[27] R. Vaidyanathan, M. Naghibosadat, S. Rauf, D. Korbie, L. G. Carrascosa, M. J. Shiddiky, M. Trau, *Anal. Chem.* **2014**, *86*, 11125.

[28] a) J. M. Lewis, A. D. Vyas, Y. Qiu, K. S. Messer, R. White, M. J. Heller, *ACS Nano* **2018**, *12*, 3311; b) S. D. Ibsen, J. Wright, J. M. Lewis, S. Kim, S.-Y. Ko, J. Ong, S. Manouchehri, A. Vyas, J. Akers, C. C. Chen, *ACS Nano* **2017**, *11*, 6641.

[29] a) M. Macka, P. Andersson, P. R. Haddad, *Anal. Chem.* **1998**, *70*, 743; b) E. Borberg, M. Zverzhinetsky, A. Krivitsky, A. Kosloff, O. Heifler, G. Degabli, H. P. Soroka, R. S. Fainaro, L. Burstein, S. Reuveni, H. Diamant, V. Krivitsky, F. Patolsky, *Nano Lett.* **2019**, *19*, 5868; c) J. Lim, M. Choi, H. Lee, J.-Y. Han, Y. Cho, *Front. Chem.* **2019**, *6*, 664.

[30] V. Krivitsky, B. Filanovsky, T. Bourenko, E. Granot, A. Praiz, F. Patolsky, *Anal. Chem.* **2019**, *91*, 14375.

[31] a) V. Krivitsky, B. Filanovsky, V. Naddaka, F. Patolsky, *Anal. Chem.* **2019**, *91*, 5323; b) E. Borberg, E. Granot, F. Patolsky, *Nat. Commun.* **2022**, *13*, 6375.

[32] Y. Sun, M. Yanagisawa, M. Kunimoto, M. Nakamura, T. Homma, *Spectrochim. Acta A: Mol. Biomol. Spectrosc.* **2017**, *184*, 1.

[33] a) M. Knepper, T. Pisitkun, *Kidney Int.* **2007**, *72*, 1043; b) Q. Zhu, L. Cheng, C. Deng, L. Huang, J. Li, Y. Wang, M. Li, Q. Yang, X. Dong, J. Su, *Proc. Natl. Acad. Sci. USA* **2021**, *118*, e2108876118.

[34] a) H. Zhou, P. S. Yuen, T. Pisitkun, P. A. Gonzales, H. Yasuda, J. W. Dear, P. Gross, M. A. Knepper, R. A. Star, *Kidney Int.* **2006**, *69*, 1471; b) J. Street, E. Koritzinsky, D. Glispie, R. Star, P. Yuen, *Adv. Clin. Chem.* **2017**, *78*, 103.

[35] a) L. He, D. Zhu, J. Wang, X. Wu, *Int. J. Mol. Med.* **2019**, *43*, 83; b) P. A. Gonzales, H. Zhou, T. Pisitkun, N. S. Wang, R. A. Star, M. A. Knepper, P. S. Yuen, *The Urinary Proteome: Methods and Protocols* (Ed: A. J. Rai), Springer, Totowa, NJ, USA **2010**, p. 89.

[36] a) M. Mathieu, N. Névo, M. Jouve, J. I. Valenzuela, M. Maurin, F. J. Verweij, R. Palmulli, D. Lankar, F. Dingli, D. Loew, *Nat. Commun.* **2021**, *12*, 4389; b) J. Kowal, G. Arras, M. Colombo, M. Jouve, J. P. Morath, B. Primdal-Bengtson, F. Dingli, D. Loew, M. Tkach, C. Théry, *Proc. Natl. Acad. Sci. USA* **2016**, *113*, E968.

[37] H. Choi, J. Y. Mun, *Appl. Microsc.* **2017**, *47*, 171.

[38] B. F. Hettich, J. J. Bader, J. C. Leroux, *Adv. Healthcare Mater.* **2022**, *11*, 2100047.

[39] C. Huang, K. P. Fisher, S. S. Hammer, J. V. Busik, *Int. J. Mol. Sci.* **2020**, *21*, 1693.

[40] a) A. Clayton, S. Al-Taei, J. Webber, M. D. Mason, Z. Tabi, *J. Immunol.* **2011**, *187*, 676; b) C. Klemann, L. Wagner, M. Stephan, S. von Hörsten, *Clin. Exp. Immunol.* **2016**, *185*, 1.

[41] A. Gámez-Valero, M. Monguió-Tortajada, L. Carreras-Planella, M. Franquesa, K. Beyer, F. E. Borràs, *Sci. Rep.* **2016**, *6*, 33641.

[42] a) L. Dong, R. C. Zieren, K. Horie, C. J. Kim, E. Mallick, Y. Jing, M. Feng, M. D. Kuczler, J. Green, S. R. Amend, *J. Extracell. Vesicles* **2020**, *10*, e12044; b) G. Vergauwen, B. Dhondt, J. Van Deun, E. De Smedt, G. Berx, E. Timmerman, K. Gevaert, I. Miinalainen, V.

Cocquyt, G. Braems, *Sci. Rep.* **2017**, *7*, 2704; c) A. H. Gheinani, M. Vögeli, U. Baumgartner, E. Vassella, A. Draeger, F. C. Burkhard, K. Monastyrskaya, *Sci. Rep.* **2018**, *8*, 3945.

[43] M. Jørgensen, R. Bæk, S. Pedersen, E. K. Søndergaard, S. R. Kristensen, K. Varming, *J. Extracell. Vesicles* **2013**, *2*, 20920.

[44] a) J. Cabral, A. E. Ryan, M. D. Griffin, T. Ritter, *Adv. Drug Delivery Rev.* **2018**, *129*, 394; b) S. A. Eming, P. Martin, M. Tomic-Canic, *Sci. Transl. Med.* **2014**, *6*, 265sr6; c) G. C. Gurtner, S. Werner, Y. Barrandon, M. T. Longaker, *Nature* **2008**, *453*, 314.

[45] M. Wang, P. Wu, J. Huang, W. Liu, H. Qian, Y. Sun, H. Shi, *Burns Trauma* **2022**, 10.

[46] D. Li, N. Wu, *Diabetes Res. Clin. Pract.* **2022**, 109882.

[47] D. G. Greenhalgh, K. H. Sprugel, M. J. Murray, R. Ross, *Am. J. Pathol.* **1990**, *136*, 1235.

[48] a) C. Crewe, J.-B. Funcke, S. Li, N. Joffin, C. M. Gliniak, A. L. Ghaben, Y. A. An, H. A. Sadek, R. Gordillo, Y. Akgul, *Cell Metab.* **2021**, *33*, 1853; b) M. E. Kranendonk, D. P. De Kleijn, E. Kalkhoven, D. A. Kanhai, C. S. Uiterwaal, Y. Van der Graaf, G. Pasterkamp, F. L. Visseren, *Cardiovasc. Diabetol.* **2014**, *13*, 37.

[49] a) A. G. Yates, R. C. Pink, U. Erdbrügger, P. R. M. Siljander, E. R. Dellar, P. Pantazi, N. Akbar, W. R. Cooke, M. Vatish, E. Dias-Neto, *J. Extracell. Vesicles* **2022**, *11*, e12190; b) X. Zhang, D. Liu, Y. Gao, C. Lin, Q. An, Y. Feng, Y. Liu, D. Liu, H. Luo, D. Wang, *Front. Cell Dev. Biol.* **2021**, 3192; c) G. Szabo, F. Momen-Heravi, *Nat. Rev. Gastroenterol. Hepatol.* **2017**, *14*, 455.

[50] S. Eid, K. M. Sas, S. F. Abcouwer, E. L. Feldman, T. W. Gardner, S. Pennathur, P. E. Fort, *Diabetologia* **2019**, *62*, 1539.

[51] a) L. Amari, M. Germain, *Front. Mol. Neurosci.* **2021**, 247; b) A. D'Souza, A. Burch, K. M. Dave, A. Sreeram, M. J. Reynolds, D. X. Dobbins, Y. S. Kamte, W. Zhao, C. Sabatelle, G. M. Joy, *J. Controlled Release* **2021**, *338*, 505.

[52] A. Hoshino, M. Ariyoshi, Y. Okawa, S. Kaimoto, M. Uchihashi, K. Fukai, E. Iwai-Kanai, K. Ikeda, T. Ueyama, T. Ogata, *Proc. Natl. Acad. Sci. USA* **2014**, *111*, 3116.

[53] D. Szklarczyk, A. L. Gable, K. C. Nastou, D. Lyon, R. Kirsch, S. Pyysalo, N. T. Doncheva, M. Legeay, T. Fang, P. Bork, *Nucleic Acids Res.* **2021**, *49*, 10800.

[54] P. Zhupanyn, A. Ewe, T. Büch, A. Malek, P. Rademacher, C. Müller, A. Reinert, Y. Jaimes, A. Aigner, *J. Controlled Release* **2020**, *319*, 63.

[55] a) A. Scomparin, D. Polyak, A. Krivitsky, R. Satchi-Fainaro, *Biotechnol. Adv.* **2015**, *33*, 1294; b) A. Krivitsky, D. Polyak, A. Scomparin, S. Eliyahu, A. Ori, S. Avkin-Nachum, V. Krivitsky, R. Satchi-Fainaro, *Biomacromolecules* **2016**, *17*, 2787.

[56] A. Krivitsky, V. Krivitsky, D. Polyak, A. Scomparin, S. Eliyahu, H. Gibori, E. Yeini, E. Pisarevsky, R. Blau, R. Satchi-Fainaro, *Polymers* **2018**, *10*, 548.

[57] H.-K. Woo, Y. K. Cho, C. Y. Lee, H. Lee, C. M. Castro, H. Lee, *Theranostics* **2022**, *12*, 1988.

[58] J. P. Landry, Y. Fei, X. Zhu, *Assay Drug Dev. Technol.* **2012**, *10*, 250.

[59] P. C. Pinheiro, A. L. Daniel-da-Silva, D. S. Tavares, M. P. Calatayud, G. F. Goya, T. Trindade, *Materials* **2013**, *6*, 3213.

[60] M. B.-Y. Greenwald, C. Tacconi, M. Jukic, N. Joshi, P. Hiebert, J. Brinckmann, H. Tenor, R. Naef, S. Werner, *J. Investig. Dermatol.* **2021**, *141*, 415.

[61] T. Stefka, T. Tikira, S. Pavel, C. Arthur, *Nat. Methods* **2016**, *13*, 731.

[62] D. Szklarczyk, A. L. Gable, K. C. Nastou, D. Lyon, R. Kirsch, S. Pyysalo, N. T. Doncheva, M. Legeay, T. Fang, P. Bork, *Nucleic Acids Res.* **2021**, *49*, D605.